

서남극 퇴적물 미세조직의 현미경 관찰을  
통한 퇴적과정과 기후변화 연구

Depositional Process and Climate Change through  
the Microscopic Observation of Sediment Microfabric  
in the West Antarctica



부산대학교

# 제 출 문

극지연구소장 귀하

본 보고서를 “과거 온난기의 서남극 빙상 후퇴 및 해양 순환 변화 연구” 과제의 위탁연구 “서남극 퇴적물 미세조직의 현미경 관찰을 통한 퇴적과정과 기후변화 연구” 과제의 단계보고서로 제출합니다.



(본과제) 총괄연구책임자 : 유 규 철  
위탁연구기관명 : 부 산 대 학 교  
위탁연구책임자 : 김 부 근  
위탁참여연구원 : 하 상 범  
“ : 양 주 연  
“ : 유 수 빈

## 보고서 초록

위탁연구과제명	서남극 퇴적물 미세조직의 현미경 관찰을 통한 퇴적과정과 기후변화 연구				
위탁연구책임자	김 부 근	해당단계 참여연구원수	4	해당단계 연구비	50,000,000
연구기관명 및 소속부서명	부산대학교		참여기업명		
국제공동연구	상대국명 :		상대국연구기관명 :		
요약(연구결과를 중심으로 개조식 500자 이내)				보고서 면수	74
<ul style="list-style-type: none"> <li>- 북서로스해의 중앙분지에서 채취한 코아 LC42는 IRD가 빈약한 생교란 사질머드, IRD가 풍부한 괴상의 머드와 8개의 층리 머드층이 약 1백만년 동안의 퇴적을 기록함</li> <li>- 층리 머드층은 밝은 층리와 어두운 층리가 교차 반복하는 뚜렷하게 다른 구성이 특징됨</li> <li>- 현미경 관찰 및 후산란 전자영상에 의하면 밝은 층리는 쇄설성의 각진 실트입자들과 규조 파편들 그리고 화석이 포함된 머드가 모래크기로 침식된 덩어리로 구성됨</li> <li>- 어두운 층리는 주로 쇄설성 점토와 생물기원 점토입자로 구성됨</li> <li>- 코아 LC42의 층리 머드는 남극 대륙주변부의 전형적인 층리 쇄설성 머드, 층리 생규질 머드 또는 빙하기 콘투라이트와는 다르게 형성됨</li> <li>- 코아 LC42의 층리 머드는 빙하기 동안 반진조된 규조가 풍부한 이전의 퇴적층을 전진하며 침식시키는 빙상 아래에서 용융수에 의해 퇴적되는 것으로 해석됨</li> <li>- 층리 머드의 대부분의 생물 구성물질은 이전 퇴적층에서 재퇴적된 것으로 퇴적 당시의 생산성 증가와는 관련이 없음</li> <li>- 층리 머드내의 황철석의 발견은 머드 퇴적동안 저층수의 용존산소가 적었음을 지시함</li> <li>- 빙해양 층리 머드의 기원과 고기후 고해양 의미를 해석하는 경우 생물 기원 물질의 재순환을 특별하게 고려해야 함</li> </ul>					
색 인 어 (각 5개 이상)	한 글	남극해, 기후변화, 고환경, 퇴적물, 미세조직			
	영 어	Southern Ocean, Climate Change, Paleoenvironment, Sediments, Microfabric			

# 요 약 문

## I. 제 목

- 서남극 퇴적물 미세조직의 현미경 관찰을 통한 퇴적과정과 기후변화 연구

## II. 연구개발의 목적 및 필요성

- 북서로스해의 중앙분지에서 새로운 빙해양 층리머드의 퇴적 발표
- 중앙로스해의 힐라리협곡 동쪽의 대륙사면 및 대륙대에서 채취한 세 개의 시추코아 퇴적물 연구

## III. 연구개발의 내용 및 범위

- 퇴적물의 조직, 구성 및 구조의 다양한 관찰을 통한 퇴적동안의 퇴적과정과 조건을 해석
- 해양과 빙상 사이의 상호관계를 규명하기 위하여 플라이스토세 층리머드의 고기후학적 의미를 토의
- 다양한 자료를 이용하여 빙하기동안 로스해 빙상의 발달에 대한 힐라리협곡 동쪽의 대륙사면과 대륙대의 증가된 퇴적물에 대한 빙해양 퇴적과정 이해

## IV. 연구개발결과

- 북서로스해의 중앙분지에서 채취한 코아 LC42는 IRD가 빈약한 생교란 사질머드, IRD가 풍부한 피상의 머드와 8개의 층리 머드층이 약 1백만년 동안의 퇴적을 기록함
- 현미경 관찰 및 후산란 전자영상에 의하면 밝은 층리는 쇄설성의 각진 실트입자들과 규조과편들 그리고 화석이 포함된 머드가 모래크기로 침식된 덩어리로 구성된 반면에 어두운 층리는 주로 쇄설성 점토와 생물기원 점토입자로 구성됨

- 코아 LC42의 층리 머드는 남극 대륙주변부의 전형적인 층리 쇄설성 머드, 층리 생규질 머드 또는 빙하기 콘투라이트와는 다르게 형성됨
- 코아 LC42의 층리 머드는 빙하기 동안 반건조된 규조가 풍부한 이전의 퇴적층을 전진하며 침식시키는 빙상 아래에서 용융수에 의해 퇴적되는 것으로 해석됨
- 코아 LC42의 층리 머드의 대부분의 생물 구성물질은 이전 퇴적층에서 재퇴적된 것으로 퇴적 당시의 생산성 증가와는 관련이 없음
- 코아퇴적물에서 측정된 방사성탄소동위원소의 연대와 관계없이 분석된 자료에 근거하여 퇴적상은 A, B1, B2로 구분되고 각각 홀로세, 후빙기 그리고 빙하기를 지시함
- 코아퇴적물의 퇴적률은 수심이 증가하면서 감소하며 홀로세(A층)보다 후빙기(B1층)에서 증가함
- 코아퇴적물의 생물생산성 지시자들은 간빙기 A층보다 빙하기 B2층에서 더 높게 나타나고 후빙기 B1층은 전이적인 값을 보임
- 코아퇴적물 B2층의 높은 생물기원물질 함량은 로스빙상이 전진하며 빙상아래에 대륙붕퇴적물을 침식 재동시켜서 대륙사면과 대륙대에 퇴적물 운반을 증가시킨 결과임

#### V. 연구개발결과의 활용계획

- 남극해 다른 지역의 심부시추 사업을 통해 획득된 자료의 장기 역사의 해석을 위한 기초자료로 활용
- 국제학술지 논문 작성을 위한 자료로 활용

# S U M M A R Y

## (영 문 요 약 문)

### I. Title

- Depositional process and Climate Change through the Microscopic Observation of Sediment Microfabric in the West Antarctica

### II. Purpose and Necessity of R&D

- To report a previously undocumented type of glaciomarine laminated muds from the Central Basin of the northwestern Ross Sea
- To investigate three sediment cores that were collected across the continental slope and rise on the east of Hillary Canyon in the central Ross Sea

### III. Contents and Extent of R&D

- To interpret the depositional processes and conditions during their formation, based on the macro- to microscopic observations of sediment texture, componentry, and structure
- To discuss the paleoclimatic implications of these Pleistocene laminated muds to shed light on the interplay between the ocean and the ice sheet
- To understand the glaciomarine depositional processes related to the RIS, emphasizing the enhanced re-sedimentation of shelf sediments in the continental slope and rise to the east of the Hillary Canyon in response to the advance of the RIS during the glacial periods using multi-proxy

data, mainly focused on geochemical and isotope signatures

#### IV. R&D Results

- Core LC42 from the Central Basin of the northwestern Ross Sea contains eight laminated mud intervals that are intercalated with IRD (ice-rafted debris)-poor bioturbated sandy mud and IRD-rich massive mud deposited over the last 1 Ma.
- Microscopic observation and backscattered electron imagery reveal that the light laminae comprise terrigenous angular to subangular silt-sized particles, scattered diatom fragments, and eroded sand-sized lumps of fossil-bearing mud. In contrast, the dark laminae are clayey and biogenic.
- The laminated muds of LC42 are different from typical laminated terrigenous muds or biosiliceous muds and glacial contourites in the Antarctic continental margin.
- These laminated muds are interpreted to have been deposited during the glacial periods by meltwater milky plumes underneath the glaciers that advanced upon and tore off the earlier-deposited and semi-consolidated diatom-rich sediments.
- Most biogenic components of the laminated muds were recycled from older deposits, indicating that they are not related with enhanced biological production at the time of mud deposition.
- Besides older AMS  $^{14}\text{C}$  ages of bulk sediments, based on the analytical results, sediment lithology was divided into units A, B1, and B2, representing Holocene, deglacial, and glacial periods, respectively.
- The sedimentation rate decreased as the water depth increased, with a higher sedimentation rate in the deglacial period (unit B1) than the Holocene (unit A).
- Biological productivity proxies were significantly higher in glacial unit B2 than in interglacial unit A, with transitional values observed in deglacial unit B1.
- The higher biogenic contents in unit B2 are primarily attributed to the

increased transport of eroded and reworked shelf sediments that contained abundant biogenic components to the continental slope and rise beneath the advancing RIS.

#### V. Application Plans of R&D Results

- Application to the interpretation on the long-term history of ice sheet evolution by the deep-sea drilling data in the other regions of the Southern Ocean
- Utilization to prepare for the international scientific paper





# 목 차

제 1 장 서론

제 2 장 국내외 기술개발 현황

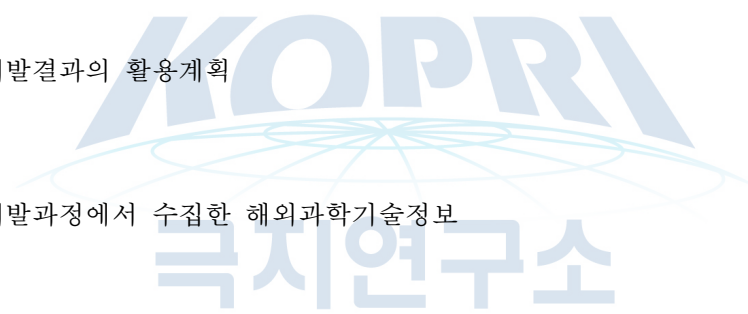
제 3 장 연구개발수행 내용 및 결과

제 4 장 연구개발목표 달성도 및 대외기여도

제 5 장 연구개발결과의 활용계획

제 6 장 연구개발과정에서 수집한 해외과학기술정보

제 7 장 참고문헌



## 제 1 장 서론

Approximately 98% of Antarctica is covered with ice; thus, the continental ice plays an important role in the global water cycle and climate change (Pattyn et al., 2018). If the entire Antarctic Ice Sheet (AIS) were to melt, the global sea level would rise as high as ~60 m above the present-day level, which is equivalent to almost half of the range that it fell during the last glacial period (Nakada et al., 2000; DeConto and Pollard, 2016). The AIS is geographically divided into the West Antarctic Ice Sheet (WAIS) and East Antarctic Ice Sheet (EAIS) by the Transantarctic Mountains. The marine-based WAIS is largely below sea level and flows rapidly, compared to the EAIS (Fretwell et al., 2013). Hence, the WAIS is more sensitive to changes in seawater temperature and sea level (DeConto and Pollard, 2016). The AIS plays an important role in controlling global climate change, with variations in the extent of the AIS affecting the surface albedo, global sea level, ocean circulation, and the production of bottom water (e.g., Ogura and Abe-Ouchi, 2001; Mackensen, 2004; Ritz et al., 2015).

The WAIS discharges ice into the central and eastern sectors of the Ross Sea, while the EAIS supplies ice to the western sector (Rignot et al., 2008). The extensive Ross Ice Sheet (RIS) primarily developed from portions of both with a comparatively higher contribution from the WAIS. The RIS advanced to the shelf edge in the eastern Ross Sea during the Last Glacial Maximum (LGM) (Fig. 1; Anderson et al., 2019, Lowry et al., 2020). Contrastingly, the RIS did not reach the shelf edge in the central and western Ross Sea, where it ceased its advance at Mawson Bank, Pennell Bank, JOIDES Basin, and the Pennell Trough during the LGM (Fig. 1; Howat and Domack, 2003; Anderson et al., 2019; Prothro et al., 2020; Torricella et al., 2021). The advance and retreat of the RIS significantly influences the depositional processes and environments in the Ross Sea (Domack et al., 1999; Anderson et al., 2014; Prothro et al., 2018; Smith et al., 2019; King et al., 2022).

The Antarctic sedimentary and climate history during the last glacial period, the glacial termination, and the Holocene has been subject to extensive modeling and empirical reconstruction over the past few decades (e.g., Barker et

al., 1999; Yokoyama et al., 2000; Licht et al., 2005; Weber et al., 2011; Golledge et al., 2013; Anderson et al., 2014, 2019; Mezgec et al., 2017; Bart et al., 2018; Prothro et al., 2018; 2020; Kim et al., 2021, Melis et al., 2021; Torricella et al., 2021, King et al., 2022). The unique sedimentary successions that are associated with RIS activity on the continental shelf of the Ross Sea have thus been well established. Anderson et al., (2014) reported that diamicton was deposited extensively in the subglacial or glacial-marine setting of the continental shelf during the LGM. Diamicton or subglacial till was also found to have been deposited widely under the grounded ice sheet during the LGM (Prothro et al., 2018; Smith et al., 2019). At this time, frequent debris flows and turbidity currents from the front of the grounding line supplied large quantities of sediments to the deep basin (Barker et al., 1999; Weber et al., 2011). During the glacier retreat (i.e., transition time or deglaciation), the ice shelf and the distance from the grounding line controlled the sedimentary processes in the continental shelf (Bart et al., 2017; Prothro et al 2018). The supply of ice-rafted debris (IRD) increased and laminated sandy silt was deposited as a result of the seasonal melt-water outflow from the front of the grounding line (e.g., Smith et al., 2019). The warm climate and seasonally open marine conditions in the Holocene thus allowed a high primary productivity of diatoms in the surface water, leading to the deposition of abundant biogenic sediments (i.e., siliceous mud and ooze) on the western side of the continental shelf, while the Holocene muds on the eastern side are characterized by scarce and reworked diatoms (Langone et al, 1998; Domack et al., 1999; Melis and Salvi, 2009; Anderson et al., 2014; McGlannan et al., 2017).

The glaciomarine sedimentation on the continental slope and rise around Antarctica was also influenced by the dynamics of the AIS (Pudsey, 2000; Caburlotto et al., 2010; Kim et al., 2020; Hillenbrand et al., 2021). During the glacial period, the AIS advanced beyond the continental shelf toward the shelf edge on most of the Antarctic continental margins (e.g., the Ross Sea, the Weddell Sea, and around the Antarctic Peninsula), resulting in the transportation of eroded and unsorted sediments from the continental shelf toward the upper continental slope by melt-water (Escutia et al., 1997; Weber et al., 2011; Khim et al., 2021). The turbidity current also transported the eroded and reworked

hemipelagic sediments of the continental shelf farther onto the lower continental slope and rise (Kuvaas and Leitchenkov, 1992; Weber et al., 1994; Escutia et al., 1997; Stow and Smillie, 2020). Bottom currents formed contourite deposits on the Antarctic continental margin under the high sedimentation rates and lack of bioturbation that occurred during the glacial period (Pudsey 1992; Gilbert et al., 1998; Lucchi and Rebesco, 2007; Rebesco et al., 2014). Such depositional processes led to an increase in the sedimentation rate in the continental slope and rise (Pudsey, 2000; Weber et al., 2011; Rebesco et al., 2014; Stow and Smillie, 2020); however, evidence for the erosion and reworking of shelf sediments has not yet been reported.

Most previous studies on the continental slope and rise of the Ross Sea have examined the western part of the region (Tolotti et al., 2013; Kim et al., 2020; Kim et al., 2021; Melis et al., 2021; Torricella et al., 2021). In the Central Basin to the western of the Iselin Bank, the terrigenous sediment supply increased during the glacial period due to strong glacial influence (Torricella et al., 2021). The following deglaciation is characterized by an abrupt increase in biogenic materials consisting mainly of diatoms and silicoflagellates, which led to the maximum of primary production. Then, the Holocene period is characterized by high, albeit lower, biogenic flux (Hartman et al., 2021). The similar results were reported by Kim et al. (2020) using the two gravity cores from the western side of the Iselin Bank.

The previous studies were conducted lesser[have been carried out less] on the eastern side of Iselin Bank than on its western side. The physical properties (i.e., magnetic susceptibility, bulk density, and P-wave velocity) of the sediments comprising the continental slope on the eastern side of the bank indicate that sedimentation patterns were different between the glacial and interglacial periods (Bonaccorsi et al., 2000). For example, structureless or stratified diamicton were deposited during the glacial period, while laminated sediments that were affected by biogenic productivity were commonly deposited during the interglacial period. However, the sedimentary records are incomplete and discontinuous because the studied cores were collected from channel systems. Furthermore, the geochemical and isotope signatures of the continental slope and rise sediments on the eastern part of the Iselin Bank have not yet

been studied.

In this study, we investigated three sediment cores that were collected across the continental slope and rise on the east of Hillary Canyon in the central Ross Sea. For the first time, multi-proxy data, mainly focused on geochemical and isotope signatures, were used to understand the glaciomarine depositional processes related to the RIS, emphasizing the enhanced re-sedimentation of shelf sediments in the continental slope and rise to the east of the Hillary Canyon in response to the advance of the RIS during the glacial periods.

In this study, we also reported a previously undocumented type of glaciomarine laminated muds from the Central Basin of the northwestern Ross Sea. Based on the macro- to microscopic observations of sediment texture, componentry, and structure, we attempt to interpret the depositional processes and conditions during their formation. We also discuss the paleoclimatic implications of these Pleistocene laminated muds to shed light on the interplay between the ocean and the ice sheet.

KOPRI  
극지연구소

## 제 2 장 국내외 기술개발 현황

The Ross Sea is characterized by steep shelf edges, many north-northeast trending basins, troughs and banks (the Drygalski, JOIDES, and Glomar-Challenger basins, Pennell Trough, and the Crary, Iselin, Mawson, and Pennell banks), and a landward deepening of the continental shelf (Fig. 1). The banks are generally shallower than 500 m. The continental shelf in the Ross Sea is geographically divided into eastern and western sectors at 180°. The eastern continental shelf consists of broad basins and low-relief banks, while the western continental shelf is characterized by narrow basins and high banks (e.g., Halberstadt et al., 2016; Gales et al., 2021). The topography of the inner continental shelf has resulted from the repeated advance and retreat of the RIS, where ice streams may have flowed toward the deep basin through the many deep troughs (Livingstone et al., 2012). These ice streams advanced to the shelf edge, forming submarine canyons on the continental slope that then supplied more sediments to the continental slope and rise. The continental slope of the Ross Sea is also divided into eastern and western parts by the Iselin Bank (Fig. 1). The eastern continental slope is gentle with numerous submarine canyons, whereas the western continental slope is steep with fewer submarine canyons (Gales et al., 2021).

The water masses in the Ross Sea include the Antarctic Surface Water (AASW), Circumpolar Deep Water (CDW), Antarctic Bottom Water (AABW), and the dense shelf waters that include the Ice Shelf Water (ISW) and High Salinity Shelf Water (HSSW) (e.g., Castagno et al 2019). The CDW, which is characterized by higher temperature ( $>1.5^{\circ}\text{C}$ ) and salinity ( $>34.60\text{‰}$ ), flows along the Ross Gyre and enters into the Ross Sea via the Antarctic Slope Current (ASC), which flows westward along the continental slope following the Antarctic Slope Front (Fig. 1). Some of the CDW flows across the ASC and onto the continental shelf, where it mixes with the low temperature ( $<-1.85^{\circ}\text{C}$ ) and low salinity ( $<34.50\text{‰}$ ) AASW. The dense shelf waters (ISW and HSSW) flows in a cyclonic direction on the continental shelf and connects the grounding line of the Ross Ice Shelf with the continental slope through the troughs on the

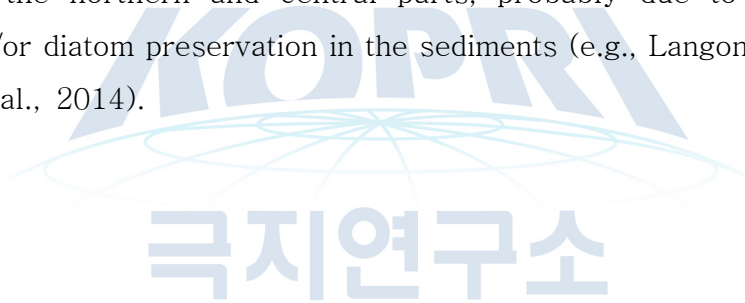
continental shelf. The HSSW is exported from the continental shelf at the northwestern corner of the Ross Sea and mixes with the CDW as it descends the continental slope, producing the AABW that then flows out into the abyssal Australian–Antarctic Basin.

The study area comprises the continental slope and rise on the eastern side of Hillary Canyon in the central Ross Sea (Fig. 1). The Hillary Canyon, developed on the continental slope and rise, is characterized by many gullies on the upper continental slope (Gales et al., 2021). The Hillary Canyon is one of the main pathways for a downslope flow of HSSW and upslope flow of CDW (Conte et al., 2021). The ASC on the continental slope carries the CDW onto the continental shelf (e.g., Smith et al., 2014; Thompson et al., 2018.). This intrusion of the CDW onto the continental shelf was blocked by the advancing ice sheet during the glacial period; however, it was still able to affect the continental slope on the eastern side of Hillary Canyon because the ASC moved northward (Gales et al., 2021).

The biogenic productivity in the surface water along the continental margin of the Ross Sea depends on both the degree of seasonal sea ice coverage and the availability of nutrient (Arrigo and van Dijken, 2004; Smith et al., 2014). The surface water is covered with sea ice during winter; thus, very low amounts of biogenic flux are supplied only from the polynya areas that form in front of the Ross Ice Shelf due to katabatic winds (Langone et al., 2000). During the period from spring to summer, the sea ice begins to disappear from the western part of the continental shelf, and phytoplankton (*Phaeocystis antarctica*) starts to bloom in the surface water (Arrigo et al., 2000). After the sea ice disappears completely, a second bloom composed of diatoms (*Fragilariopsis curta*) forms at the front of the Ross Ice Shelf, leading to the deposition of sediments comprising siliceous ooze on the continental shelf (Arrigo et al., 2000). The appearance of *F. curta* has been reported in the Glomar–Challenger Basin in the central Ross Sea and in the outer continental shelf of the Wales Deep Basin in the eastern Ross Sea (Tolotti et al., 2013; McGlannan et al., 2017).

The surface sediments on the continental shelf of the Ross Sea consist of siliceous ooze and residual glaciomarine sediments (Langone et al., 1998;

Prorthro et al., 2018). These present-day siliceous mud and ooze are associated with seasonal sea ice and polynya in the surface water (Arrigo et al., 2000; Mezgec et al., 2017). Conversely, the residual glaciomarine sediments that lie at the top of the banks were mostly deposited via the reworking of surface sediments by the strong bottom current (e.g., Prothro et al., 2018). The total organic carbon (TOC) content of the surface sediments on the present-day continental shelf of the Ross Sea is between ~0.2% and ~2.0% (Ledford-Hoffman et al., 1986; Frignani et al., 1992; Langone et al., 1998; McKay et al., 2008; Tolotti et al., 2013), while that of the continental slope/margin areas range between ~0.1% and ~0.5% (Melis et al., 2021; Kim et al., 2021). The total nitrogen (TN) content is ~0.1% and the biogenic opal content varies from ~10% to >30%. The TOC content increases alongside the biogenic opal content; however, the biogenic opal content is higher in the western part of the Ross Sea than in the northern and central parts, probably due to more diatom blooming and/or diatom preservation in the sediments (e.g., Langone et al., 1998; Anderson et al., 2014).





## 제 3 장 연구개발수행 내용 및 결과

### 1 절. Recycled biogenic components of the Pleistocene glaciomarine laminated muds in the Central Basin of the northwestern Ross Sea and their paleoclimatic implications

#### 1. Summary

Glaciomarine laminated muds around the Antarctic continental margin preserve an important marine geological record of the cryogenic paleoclimate changes related to ice sheet dynamics. Core LC42 from the Central Basin of the northwestern Ross Sea contains eight laminated mud intervals that are intercalated with IRD (ice-rafted debris)-poor bioturbated sandy mud and IRD-rich massive mud deposited over the last 1 Ma. The laminated muds are characterized by distinctly different components of the alternating light and dark laminae. Microscopic observation and backscattered electron imagery reveal that the light laminae comprise terrigenous angular to subangular silt-sized particles, scattered diatom fragments, and eroded sand-sized lumps of fossil-bearing mud. In contrast, the dark laminae are clayey and biogenic. The laminated muds of LC42 are different from typical laminated terrigenous muds or biosiliceous muds and glacial contourites in the Antarctic continental margin. These laminated muds are interpreted to have been deposited during the glacial periods by meltwater milky plumes underneath the glaciers that advanced upon and teared off the earlier-deposited and semi-consolidated diatom-rich sediments. Most biogenic components of the laminated muds were recycled from older deposits, indicating that they are not related with enhanced biological production at the time of mud deposition. In addition, occurrence of framboidal pyrites supports an oxygen-depleted bottom water condition during the mud deposition. Our study thus suggests that the recycling of biogenic particles should be considered when interpreting the origin of glaciomarine laminated muds and their

paleoclimatic and paleoceanographic implications.

## 2. Materials and Methods

The Central Basin is located at the mouth of the JOIDES Basin in the northwestern Ross Sea (Fig. 1), forming a deep semi-closed tectonic depression characterized by different morphological features, including continental slope, intra-slope basin, ponded basin, basin floor, and topographic highs. Based on the seismic stratigraphic analysis, Kim et al. (2018) reported that the sediment stacking patterns reflect distinctive glacial/interglacial changes of sediment supplies related to the ice sheet dynamics and bottom current activity.

An 11.75 m-long core RS15-LC42 (hereafter LC42) was collected in the northwestern moat (71°49.40'S, 178°34.76'E, 2084 m water depth; Fig. 1) between the small contour-parallel mounds near the right flank of the Hallett Ridge in the Central Basin using jumbo gravity coring system during the cruise of R/V *Araon* in the austral summer of 2015. Optical images of LC42 were obtained using ITRAX core scanner and X-ray radiographic images were taken on 1-cm thick sediment slabs using X-ray inspection equipment (SOFTEX W-100W).

Twenty thin and polished sections from eight intervals of laminated sediments of LC42 (Fig. 2) were prepared using a fluid displacive resin embedding technique modified from Pike and Kemp (1996). These sections were examined using Nikon polarizing microscope ( $\times 100$ –1000) and scanning electron microscope (SEM) ( $\times 100$ –10000) with backscattered electron imagery (BSEI) of JEOL (JZA-8530F PLUS) Field-Emission Electron Probe Micro-Analyzer.

## 3. Results

The sediment facies of LC42 can be divided into 1) IRD (ice-rafted debris)-poor bioturbated sandy mud, 2) IRD-rich massive mud, and 3) laminated mud (Fig. 2). These facies are arranged without any obvious order or cyclicity. It is worthy of note that the IRD-poor bioturbated sandy mud and IRD-rich massive mud overlie the laminated mud in the uppermost part of LC42. Eight

laminated mud intervals are identified with variable thicknesses (10 cm to about 2 m) and with generally sharp boundaries with the other facies. Throughout the core, laminations are very similar and devoid of IRD and bioturbation, and consist of alternating relatively thicker light laminae and relatively thinner dark laminae, which are mostly plane-parallel, locally pinch-and-swelling and low-angle inclined.

Microscopic observation of thin sections clarifies that the light and dark laminae are millimeter- to submillimeter-thick and composed mainly of silty and clayey particles, respectively (Fig. 3, Supplement Fig. S1). The contacts between these laminae are either sharp or transitional and planar to undulatory. SEM examination reveals that the fine-grained lamina consists of sparsely scattered silt-sized particles of terrigenous or biogenic origin in a clayey matrix. In contrast, the coarse-grained lamina is composed dominantly of very fine sand- to silt-sized angular to subangular quartz and feldspar grains, and contains considerable amounts of sand- to silt-sized biogenic fragments and sand-sized lumps of coagulated very small diatom fragments and clay particles (Fig. 3, Supplement Fig. S1). In addition, framboidal pyrites are observed in all laminated mud layers (Fig. 3, Supplement Fig. S2).

#### 4. Discussion

The glaciomarine laminated muds in the Central Basin seem unique in terms of depositional age, compositional variations, and depositional conditions. Despite uncertainty, LC42 accumulated over ~1 Ma that covers at least ten glacial-interglacial cycles (Ohneiser et al., 2019). The exact ages of individual laminated mud intervals are difficult to date. Nevertheless, deposition of the eight laminated mud intervals, despite the variable thicknesses, must have occurred during the repeated advance and retreat of the Ross Ice Sheet. Occurrence of the IRD-poor bioturbated sandy mud and IRD-rich massive mud intervals at the top of the core (Fig. 2) can be regarded as an indirect evidence against the deposition of the laminated mud intervals under warm conditions, suggesting laminated mud deposition without IRDs in the glacial periods. As the currently reported geological period of laminated mud deposition in the Antarctic

continental margin is limited mainly to the Holocene to the last glacial period (Stickley et al., 2005; Maddison et al., 2012; Alley et al., 2018), the laminated muds of LC42 can provide new information on the glaciomarine sedimentation in the polar slope basin over a much longer geological time span.

The laminated muds of LC42 are distinguishable from the laminated terrigenous muds and laminated biosiliceous muds, in terms of the particle compositions (Fig. 3). The lamination of LC42 is characterized by the alternations of light and dark laminae that are composed of particles from diverse origins. Albot (2016) reported that the detrital particles in these laminated muds show bimodal (silt and clay, corresponding to the light and dark laminae) grain size distribution. However, the particle composition in these laminae is unusual in that the coarse-grained light lamina contains sand-sized biogenic fragments and eroded lumps or chips of semi-consolidated diatom-rich sediments that were definitely deposited much earlier in addition to mostly very fine sand- to silt-sized angular to subangular siliciclastic particles (Fig. 3). In contrast, the clayey particles of dark lamina are dominantly composed of biogenic powders of ground fossils with very fine silt-sized biogenic fragments. Bollen (2019) reported the abundant old (Pliocene to Miocene) diatom species (e.g., *Coscinodiscus rhombicus*, *Denticulopsis hustedtii*, *Fragilariopsis arcula*, and *Thalassiosira oliverana*) from these laminated mud layers, although some archives of young diatom fossils were observed (Fig. 3). Thus, a significant portion of the sedimentary particles in the laminated muds was derived from older diatom-rich sediments that were eroded and transported by moving glaciers to the Central Basin.

During the Last Glacial Maximum, the Ross Ice Sheet did not advance to the shelf edge in the central and western Ross Sea (Hall et al., 2013; Anderson et al., 2014; Lee et al., 2017). These advance and retreat of the Ross Ice Sheet between the glacial and interglacial periods were recorded in the sedimentary sequences (coarse-grained grounding line-proximal sediments, transition from coarse- to fine-grained sediments, and open marine diatom-rich muds) in the continental shelf areas (Smith et al., 2019). During the glacial periods, the grounding line was located near the shelf edge of the northwestern Ross Sea, where the glacial activity of ice sheet had a greater influence on the

depositional condition in the continental slope and rise (Anderson et al., 2014). In general, IRD deposition increased during the warm period by increased calving and floating ice, whereas the lack of IRD seems to be due to the wide development of sea ice during the glacial period. Instead, meltwater-derived debris flows occur frequently to cause mass transport toward the continental slope proximal to the grounding lines (Anderson, 1999). Fine-grained sediments might be transported farther away from the ice-shelf zone, and glacial marine muds with well-sorted and very fine sand are deposited by basal debris settling. Other glacial fine-grained laminated sediments are deposited as contourites in the drift areas of the deep continental margin by the intensified activity of bottom current (Sprenk et al., 2014).

The absence of IRD and bioturbation in the laminated muds of LC42 in the slope basin of the Hallett Ridge suggests that the mud deposition occurred in the glacial periods. These laminated muds were deposited by the continuous supply of meltwater milky plume generated underneath the advancing glacier that contained the eroded lumps of semi-consolidated diatom-rich fossiliferous sediments. After the glacial pumping, the density-based segregation of grain size and selective settling during the continuous flow may have facilitated the formation of laminated muds. The pinch-and-swelling and low-angle inclined lamination of the light laminae with possible internal truncation surfaces and imbrication of particles (Fig. 3) suggests the mud deposition from dilute density currents. The density currents might have been fed either from the waxing and waning subglacial meltwater discharges or from buoyant suspensions associated with mass wasting processes (slide/slump and debris flows) near the grounding lines (Mulder et al., 2003; Tripsanas and Piper, 2008).

In general, the Antarctic continental margin is characterized by decreased productivity during the glacial periods, depending on the light and nutrient availability (e.g., Bonn et al., 1998). Such coupling between productivity and climate has been well observed from the sedimentary records in the Antarctic continental shelf (e.g., Frignani et al., 1998). The glacial productivity was also reduced in the Antarctic continental slope and rise due to much wider expansion of seasonal or permanent sea ice coverage (e.g., Wu et al., 2017). On the other hand, it was found recently that the deglacial and glacial sediments of the Ross

Sea continental slope and rise are characterized by higher levels of biogenic components than the Holocene sediments, which were interpreted to be due to the glacial supply of reworked diatom-rich shelf sediments (Khim et al., 2021; Ha et al., 2022). Under this situation, the application of a simplistic productivity-climate model to LC42 would lead to a wrong interpretation that the fossiliferous laminated muds represent enhanced productivity during the warm climate conditions. However, such high biogenic components of the laminated mud result from the abundant supply of either tiny fragmented and congregated diatoms during periods of increased glacier activity or even the clay-sized diatomaceous powders finely ground by advancing glaciers also during increased glacier activity. In particular, these diatoms are distinguished in that they are mostly old and reworked (Bollen, 2019), and are not related with diatom production in the surface water of the Central Basin at the time of mud deposition. Thus, the laminated muds of LC42 present insightful evidence on the Pleistocene paleoclimate in the Central Basin.

## 5. Conclusions

The light and dark laminated muds of core LC42 from the Central Basin are characterized by distinctly different componentry, distinguishable from typical laminated terrigenous muds or biosiliceous muds and glacial contourites in the Antarctic continental margin. Terrigenous silt-sized particles, scattered diatom fragments, and eroded sand-sized lumps of fossil-bearing mud are dominant in the light lamina, whereas biogenic clayey particles are enriched in the dark laminae. However, because most biogenic components of the laminated muds were recycled from older deposits, *in situ* paleoproductivity information during the mud deposition seems difficult to interpret in terms of biogenic proxies.

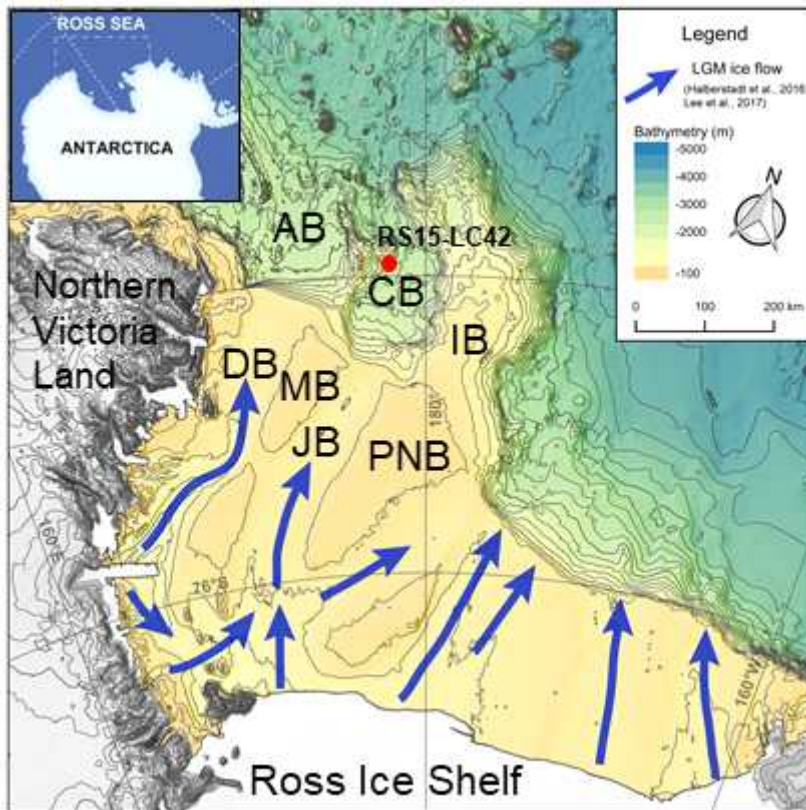


Figure 1. Bathymetric map of the Ross Sea (modified from Kim et al., 2018) with the location of core RS15-LC42. Blue arrows represent the likely LGM ice flows along the main glacial troughs on the continental shelf. AB = Adare Basin; CB = Central Basin; DB = Drygalski Basin; IB = Iselin Bank; JB = Joides Basin; MB = Mawson Bank; PNB = Pennell Bank.

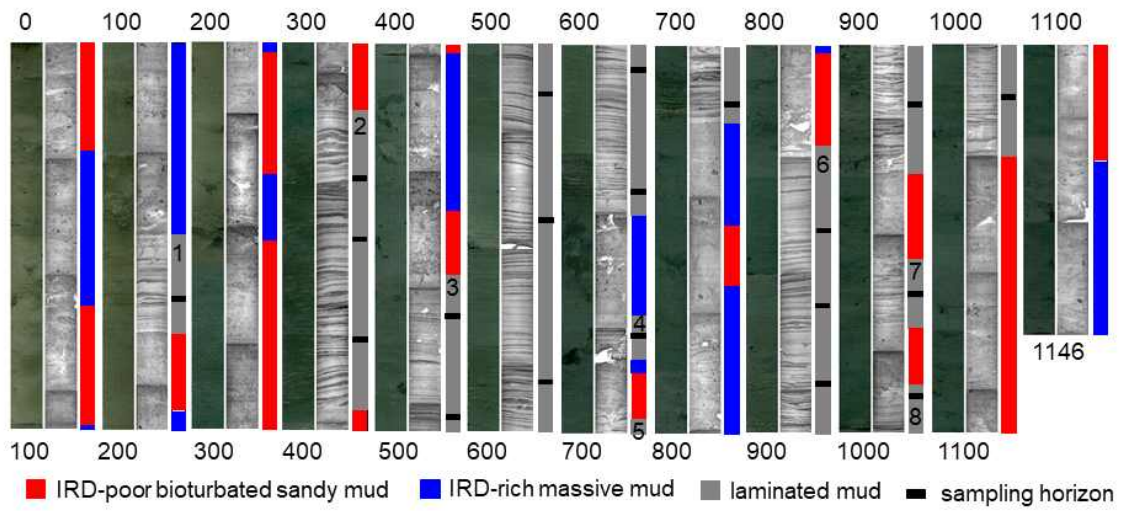


Figure 2. Core photos and X-ray photographs of core LC42, consisting of three major lithologic facies (IRD-poor bioturbated sandy mud, IRD-rich massive mud, laminated mud). Sample horizons for the thin and polished sections are indicated.





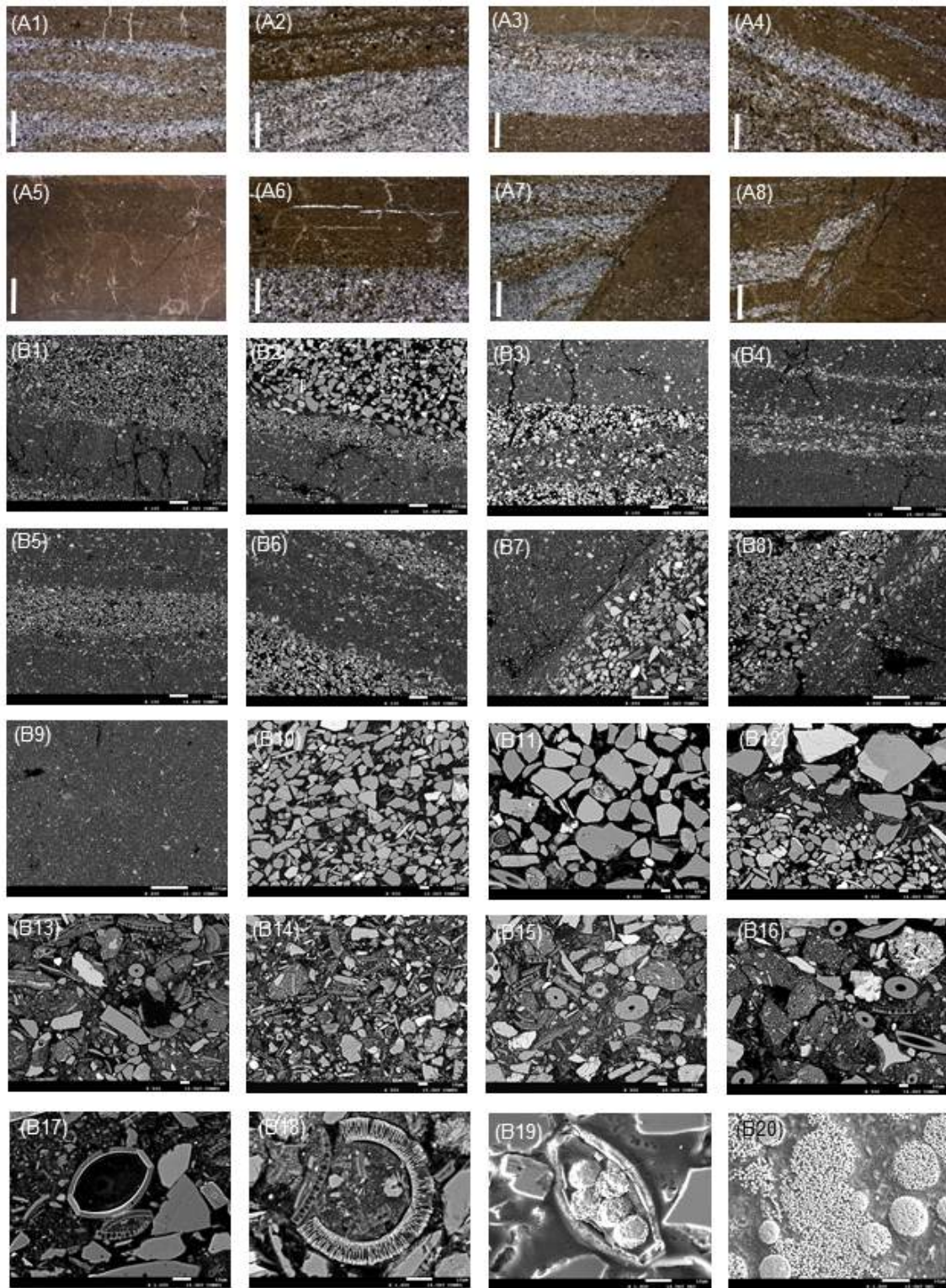


Figure 3. Photomicrographs of thin sections (A1 to A8, scale bar: 0.5 mm) and BSEI of polished sections (B1 to B20) of core LC42. A1: alternations of submillimeter-thick, light and dark laminae (TL2), A2: couple of dark and light lamina containing very thin laminae (TL4), A3: light lamina with sharp upper and lower boundaries and internal grain size variations (TL5), A4: a series of thin light and dark laminae (TL9), A5: dark clay lamina (TL12), A6: boundary between light and dark lamina (TL13), A7: dark and light lamina truncated by a microfault (TL18), A8: microfaulting of dark and light lamina (TL20), B1: typical dark and light lamina (TL10, x100, 100  $\mu$ m), B2: multiple layering of laminae with different grain sizes (TL13, x100, 100  $\mu$ m), B3: a dark lamina intercalated by light laminae (TL2, x100, 100  $\mu$ m), B4: very thin light laminae within dark lamina (TL19, x100, 100  $\mu$ m), B5: a very thin light lamina with diffuse upper and lower boundaries (TL17, x100, 100  $\mu$ m), B6: a dark lamina containing silt-sized clastic particles (TL9, x100, 100  $\mu$ m), B7: microfault surface between dark and light lamina (TL18, x200, 100  $\mu$ m), B8: light and dark laminae bounded by a microfault (TL20, x200, 100  $\mu$ m), B9: massive clay-rich dark lamina (TL12, x200, 100  $\mu$ m), B10: close-up of fine silt-sized particles in the light lamina (TL1, x500, 10  $\mu$ m), B11: close-up of coarse silt-sized particles in the light lamina (TL9, x500, 10  $\mu$ m), B12: inverse grading of coarse particles (TL13, x500, 10  $\mu$ m), B13–B16: close-up of mixed terrigenous and biogenic sediment lumps or aggregates containing tiny biogenic fragments (TL4, TL7, TL8, TL13, x500, 10  $\mu$ m), B17: archived diatom fossil and fragments (TL2, x1000, 10  $\mu$ m), B18: fossil containing the biogenic fragments (TL8, x1400, 10  $\mu$ m), B19: framboidal pyrites within diatom fossil (TL13, x1400, 10  $\mu$ m), B20: pyrite patches (TL20, x1500, 10  $\mu$ m). For the position of TL and further relevant photos, please see Supplement Figure S3 and S4.

## 2 절. Glaciomarine sediment deposition on the continental slope and rise of the central Ross Sea since the Last Glacial Maximum

### 1. Summary

The continental margin of the Ross Sea has been consistently sensitive to the advance and retreat of the Ross Ice Sheet (RIS) between the interglacial and glacial periods. This study examines changes of the glaciomarine sedimentation on the continental slope and rise to the eastern side of Hillary Canyon in the central Ross Sea, using three gravity cores collected at increasing water depths. Besides older AMS  $^{14}\text{C}$  ages of bulk sediments, based on the analytical results, sediment lithology was divided into units A, B1, and B2, representing Holocene, deglacial, and glacial periods, respectively. The sedimentation rate decreased as the water depth increased, with a higher sedimentation rate in the deglacial period (unit B1) than the Holocene (unit A). Biological productivity proxies were significantly higher in glacial unit B2 than in interglacial unit A, with transitional values observed in deglacial unit B1. Biological productivity generally decreased in the Antarctic continental margin during the glacial period because of extensive sea ice coverage. The higher biogenic contents in unit B2 are primarily attributed to the increased transport of eroded and reworked shelf sediments that contained abundant biogenic components to the continental slope and rise beneath the advancing RIS. Thus, glacial sedimentation on the continental slope and rise of the central Ross Sea was generally governed by the activity of the RIS, which generated melt-water plumes and debris flows at the front of the grounding line, although the continental rise might have experienced seasonally open conditions and lateral effects due to the bottom current.

### 2. Materials and Methods

Three gravity cores (GC1, GC2, and GC3) and three box cores (BC1, BC2, and BC3) were obtained at three stations (RS14-C1, C2, and C3) across the

continental slope and rise on the east of Hillary Canyon (central Ross Sea) during the XXIX Italian PNRA (National Antarctic Research Program) Expedition (PNRA-ENEA/UTA, 2014) under the Italian project ROSSLOPE II (Fig. 1, Table 1). The box cores were used to check the extent of loss from the gravity cores and the core-top age, whereas the gravity cores were used to reconstruct the changes in glaciomarine sedimentation. The obtained cores were split, visually described, and photographed at the University of Trieste (Italy). The box cores and the upper parts (core-top to 34 cm in GC2 and to 38 cm in GC3 and GC1) of gravity cores were sampled at every 4 cm intervals, whereas the lower parts of the gravity cores (rest of the core sections to the core-bottom) at every 8 cm intervals. All analytical data are summarized in Supplementary Data File.

Magnetic susceptibility (MS) measurements were conducted using a 2G cryogenic magnetometer equipped with a Bartington magnetic susceptibility meter at 1 cm interval in the paleomagnetic laboratory of the Istituto Nazionale di Geofisica e Vulcanologia (INGV, Italy). Samples for grain size analyses were treated with hydrogen peroxide in order to remove the organic matter and the remaining sediments were sieved using a 2-mm sieve. The biogenic silica and carbonate were not eliminated due to the abundance of the siliciclastic particles, which preserve the non-biogenic silica component (glass ash or IRD) derived from glacial abrasion. Chemical treatment for the removal of biogenic silica can damage the terrigenous silica components (e.g., McCave and Andrews., 2019). Sediment particle sizes (<2 mm) were determined using a Malvern Mastersizer Hydro2000S diffraction laser unit at the University of Trieste (Italy). Sand, silt, and clay fractions were classified according to the scheme of Friedman and Sanders (1978). Because the diatom abundance and carbonate content were quite low, the inclusion of these components would not strongly bias the analytical results of grain size. Further, the proportional trend among sand, silt, and clay may be similar under removed and unremoved conditions, although the absolute content was different in each component. In this study, the coarse particles (sand and IRD) that were used to interpret the depositional processes were not affected by the overestimated silt content. Particles with sizes >2 mm were counted. Preliminary mineral composition identification of IRD was carried out at

a depth of 38 cm (i.e., the horizon with the highest amount of IRDs) in GC3, with several IRD samples powdered for observation using an X-ray diffractometer (XRD; Siemens/Brucker D5005). Selected grains were photographed and examined using a scanning electron microscope-energy dispersive spectrometry (SEM-EDS) analyzer (JSM-6380LV) at Gyeongsang National University (Korea).

The sediment samples were then freeze-dried and powdered for geochemical analyses at Pusan National University (Korea). Total carbon (TC) and TN contents were measured using a CHN elemental analyzer (Flash 2000 Model) with an analytical error of  $\pm 0.1\%$ . Total inorganic carbon (TIC) was measured using a UIC CO<sub>2</sub> Coulometer (CM5014 Model), with an analytical error of  $\pm 0.1\%$ . Calcium carbonate (CaCO<sub>3</sub>) content was calculated by multiplying the TIC content by 8.333. TOC was calculated by subtracting TIC from TC. The C/N ratio was calculated by dividing the TOC by TN. The biogenic silica content was analyzed using the wet alkaline extraction method (DeMaster, 1981) with the analytical precision measured using relative standard deviation ( $\pm 1\sigma$ ) at 1%. The biogenic opal content was calculated by multiplying the biogenic silica concentration by 2.4 (Mortlock and Froelich, 1989).

The carbon isotopic composition ( $\delta^{13}\text{C}$ ) of the carbonate-free sediments and nitrogen isotopic composition ( $\delta^{15}\text{N}$ ) of bulk sediments were measured using a Finnigan Delta Plus XP mass spectrometer directly coupled with a Thermo Fisher Scientific FLASH 2000 isotope ratio mass spectrometer elemental analyzer at Istituto di Scienze Polari-Consiglio Nazionale delle Ricerche (ISP-CNR, Italy). All isotopic compositions were expressed in conventional  $\delta$  notation and reported as parts per thousand (‰):

$$\delta^{13}\text{C} = [({}^{13}\text{C}/{}^{12}\text{C})_{\text{sample}} / ({}^{13}\text{C}/{}^{12}\text{C})_{\text{VPDB}} - 1] \cdot 10^3$$

$$\delta^{15}\text{N} = [({}^{15}\text{N}/{}^{14}\text{N})_{\text{sample}} / ({}^{15}\text{N}/{}^{14}\text{N})_{\text{air}} - 1] \cdot 10^3$$

As determined from the routine repeat measurements of the reference sample IAEA-CH7 (polyethylene,  $-32.15\%$  vs. Vienna Peedee Belemnite, VPDB), uncertainties were lower than  $\pm 0.5\%$ . The internal standard for  $\delta^{15}\text{N}$  measurements, IAEA-N-1 (ammonium sulfate,  $+0.4\%$  vs. air) was used and the error for repeated analyses of the standard was  $\pm 0.2\%$ .

Accelerator mass spectrometry (AMS) was used for  $^{14}\text{C}$  dating the

core-tops of the box cores (BC1, BC2, and BC3) and four horizons in each gravity core (GC1, GC2, and GC3) (Table 2). Due to the scarcity of foraminifera in the studied samples, the AMS  $^{14}\text{C}$  activity of the sediments was measured using the acid-insoluble organic matter (AIOM) of the bulk sediments at the Poznań Radiocarbon Laboratory of Adam Mickiewicz University (Poland) and MICADAS (Wacker et al., 2013) at the AWI (Mollenhauer et al., 2021) (Germany). Results for AMS  $^{14}\text{C}$  that are obtained using the AIOM fraction of bulk sediments are often compromised by contamination from older carbon derived from glacial erosion and/or the reworking of unconsolidated sediments (e.g. Andrews et al., 1999; Pudsey et al., 2006; Mezgec et al., 2017; Tesi et al., 2020). The AIOM ages of the core-top (0–1 cm) of BC01, BC02, and BC03 were used to correct the ages of the deeper parts of each gravity core. These ages embed the regional marine reservoir effect (MRE) and the local dead carbon contamination offset (LCO). Before calibrating the  $^{14}\text{C}$  ages, the LCO obtained for the study area was subtracted from the AIOM  $^{14}\text{C}$  box core ages (LCO-corrected ages), assuming that neither the MRE nor the LCO changed during the Holocene and the glacial periods (see Hall et al., 2010; Hillenbrand et al., 2010). The LCO-corrected AMS  $^{14}\text{C}$  ages were then converted into calibrated ages using CALIB REV 7.1 (Stuiver et al., 2018) at a 95% confidence level. The MARINE 13 calibration curve (Reimer et al., 2013) was then produced by assuming the regional marine offset ( $\Delta R$ ) to be  $0.79 \pm 0.12$  ka from the global MRE (Hall et al., 2010). The new calibration curve (MARINE 20) was not used because it is not suitable for the calibration of Antarctic sediments (Heaton et al., 2020). The uncorrected and calibrated AMS  $^{14}\text{C}$  ages are summarized in Table 2. All ages reported in this study are calibrated ages (cal. yr BP), unless otherwise specified. The calibrated  $^{14}\text{C}$  ages of the three gravity cores do not show age reversal except for one result of GC1, indicating the reasonable establishment of a sequential stratigraphic order that corresponds to the lithologic units. Although the  $^{14}\text{C}$  dating on the AIOM leads to some uncertainties in age determination widely discussed (Andrews et al., 1999; Mezgec et al., 2017; Tesi et al., 2020), the  $^{14}\text{C}$  age data in this study are consistent with the results reported previously by Andrews et al. (1999).

### 3. Results

#### 3.1. Core-top comparison

A fair amount of material from the top of gravity cores was lost during the coring process. The geochemical properties of the box core and the upper part of the gravity core were compared to estimate the core-top loss. Figure 2 shows a comparison of TOC, TN, and CaCO<sub>3</sub> contents between the two cores, for which the variation patterns were found to coincide. Differences of <0.06% for TOC, <0.01% for TN, and <0.2% for CaCO<sub>3</sub> were obtained for the core-tops at sites C1 and C2, while those of 0.3% for TOC, 0.02% for TN, and 2% for CaCO<sub>3</sub> were observed at site C3. Most of these differences were within the analytical error range. Based on this comparison, it was estimated that a few centimeters of sediment were lost from the core-top of the gravity cores. The differences in the core-top ages between BC2 and GC2 was greater (~5100 yr) than that for the other two cores (Table 2). In the case of GC2, the estimated core-top loss was ~5 cm based on the calculation of the sedimentation rate in the upper part. No high-resolution study was conducted for the Holocene; however, features describing the glacial, deglacial and interglacial periods were estimated by sedimentological and geochemical analyses. Thus, we consider that the loss of some core-top sediments is not a critical problem. Such minor loss suggests that the core-tops of the gravity cores were well preserved and that a record of the late to latest Holocene period is available, despite the relatively old <sup>14</sup>C ages (Table 2).

#### 3.2 Lithologic units (A, B1, and B2) and their occurrence in each gravity core

Based on the sediment color, core description, and analytical properties, the lithology of the three gravity cores was divided into two main units (A and B), and lithologic unit B was further divided into two subunits (B1 and B2) (Fig. 3). Lithologic unit A is characterized by brownish hemipelagic silty mud, enriched IRDs (~14 #/cm<sup>3</sup> in GC3 and ~5 #/cm<sup>3</sup> in GC2 and GC1), and high sand fraction (from 9% in GC1 to 32% in GC3) with high fluctuations in the MS (Fig. 3). The amount of IRD and the sand content of unit A decreased away from the shelf margin toward the continental rise (Fig. 3). The MS appears to

depend on the amount of IRD and the sand content.

Grayish sediment is common in unit B, however, the lithologic features of units B1 and B2 differed considerably. Unit B1 consisted of sandy mud, whereas unit B2 was composed of hemipelagic silty mud with sparse/scattered IRDs (Fig. 3). An upward increase in the IRD and sand fraction was observed in unit B1, with the MS peak at the top. In contrast, unit B2 contained very rare to sparse IRD ( $2\sim4 \text{ \#/cm}^3$ ) and low sand fractions ( $\sim 13\%$ ), with more IRDs in the lower part.

Characteristic mineral and elemental compositions were obtained from a representative IRD in GC3 (Fig. 4). The IRDs mainly consists of quartz and mica with accessory chlorite, kaolinite, plagioclase, and muscovite (Fig. 4a). A distinct peak indicating the presence of hornblende was observed at the 38 cm horizon, which also contained abundant mica. According to SEM-EDS analysis (Fig. 4b), the IRD grains were enriched in Si and Al, confirming that the dominant mineral composition was aluminosilicate. Another interesting feature was the detection of a Ca peak in some grains, which may be attributed to carbonate minerals. However, no distinct calcite peak was detected in the XRD studies, presumably because of its very low content. Nevertheless, the high  $\text{CaCO}_3$  content ( $\sim 8\%$ ) at this horizon of GC3 might be due to the occurrence of detrital grains.

The bulk and isotope geochemistry of unit A generally revealed low biogenic opal ( $3.6\sim 5.4\%$ ), TOC ( $0.16\sim 0.22\%$ ),  $\delta^{13}\text{C}$  ( $-25.2$  to  $-24.7\%$ ),  $\text{CaCO}_3$  ( $0.2\sim 0.3\%$ ), and C/N ratio ( $6.7\sim 9.1$ ), with slightly high TN ( $\sim 0.03\%$  in GC3 and GC2) and  $\delta^{15}\text{N}$  ( $4.6$  to  $4.9\%$ ) (Fig. 6). Units B1 and B2 could be also distinguished by their bulk and isotope geochemistry. Unit B2 was characterized by a lower TN ( $\sim 0.02\%$ ) and  $\delta^{15}\text{N}$  ( $3.8\%$  to  $4.9\%$ ) and higher biogenic opal ( $\sim 11.0\%$ ), TOC ( $0.30\sim 0.36\%$ ),  $\delta^{13}\text{C}$  ( $-24.8\%$  to  $-24.6\%$ ), and  $\text{CaCO}_3$  ( $\sim 1.7\%$  in GC3 and GC2 and  $\sim 0.3\%$  in GC1). Conversely, unit B1 was characterized by transitional values between those of units B2 and A, i.e., biogenic opal ( $11.1\sim 5.0\%$ ), TOC ( $0.33\sim 0.19\%$ ),  $\delta^{13}\text{C}$  ( $-24.7\%$  to  $-24.8\%$ ),  $\text{CaCO}_3$  ( $1.2\sim 0.2\%$ ), TN ( $0.02\sim 0.03\%$ ), and  $\delta^{15}\text{N}$  ( $4.5\%$  to  $4.7\%$ ) (Fig. 5).

The three gravity cores (GC3, GC2, and GC2) showed the same lithologic succession (units A, B1, and B2) (Fig. 3). GC3 consisted of the three units (A,



B1, and B2). In addition to these units, GC2 had an additional very thin layer (comprising 10 cm) of unit A at the bottom of the core. Contrastingly, the same lithologic sequence (A, B1, and B2) was repeated 3 times in GC1. The lithological boundary is not certain and its position can be shifted up or down by correlating the sites. In addition, the age of older units below the uppermost set in GC1 could not be dated. Thus, in this study, the comparison among the lithologic units is concerned with the uppermost sets of unit A (Holocene), B1 (deglacial), and B2 (glacial). Downcore geochemical and isotopic profiles of the three gravity cores confirmed the configuration and succession of the lithologic units within them (Fig. 6). Despite the different contents, the variation patterns in the geochemical and isotopic results for each lithologic unit were similar among the three cores.

#### 4. Discussion

##### 4.1. Sediment deposition on the continental slope and rise of the central Ross Sea

The core-top ages for GC3, GC2, and GC1 were found to be 1.5 ka, 5.7 ka, and 2.5 ka, respectively (Table 2). Such old ages are generally observed in core-tops from the Antarctic Ocean (Licht et al., 1996; Andrews et al., 1999). The older AMS  $^{14}\text{C}$  ages at the core-top sediments of box cores and gravity cores are due to a combination of the old carbon effect in the seawater and surface sediment loss during coring operation. The old carbon effect depends on the inclusion of old "particulate" organic carbon by the erosion of surface sediments or resuspended materials transported by lateral advection. Each site is characterized by a different proportion between old and new organic carbon. Our results show that three sites, despite very close, date the different ages of the core-top. Based on the comparison of geochemical properties with these older AMS  $^{14}\text{C}$  ages, the uppermost part of the three gravity cores should represent the Holocene accumulation, rendering lithologic unit A an interglacial sediment. Consequently, lithologic unit B, which underlies unit A, represents the deglacial and glacial (B1 and B2, respectively) sediments, based on their depositional order (Fig. 5). The old AMS  $^{14}\text{C}$  ages in unit B1 mainly occurred due to the

redeposition of old sediments onto the continental slope and rise by turbidity currents or mass accumulation processes during the deglacial period (e.g., Pudsey, 2000). Recently, Khim et al. (2021) reported that the deglacial sediments in the Central Basin of the northwestern Ross Sea were found to be older than expected by AMS  $^{14}\text{C}$  dating due to the transportation of old shelf sediments. The high IRD content and physical characterization may be related to a deglacial period with strong iceberg transit in close proximity to a calving zone. Although GC3 includes both units A and B, a complete interglacial–glacial cycle may not be recorded in this section, as compared to GC2 and GC1, which show repeated lithologic successions.

The sedimentation rate of unit A decreases prominently with an increasing water depth (6.3 cm/kyr at GC3, 2.0 cm/kyr at GC2, and 1.2 cm/kyr at GC1). In general, the supply of terrigenous sediments and biogenic productivity decreases further from the Antarctic coastal regions (Grobe and Mackensen, 1992; Domack et al., 1999; Pudsey., 2000; Arrigo et al., 2004; Prothro et al., 2018). Thus, the lowered Holocene sedimentation rate with the increasing water depth is typical because the continental shelf of the Ross Sea lay at a further distance from the continental slope and rise. Similar to unit A, the sedimentation rate of unit B1 (~9.0 cm/kyr at GC3, 2.6 cm/kyr at GC2, and 1.7 cm/kyr at GC1) also decreases with increasing water depth. However, it should be noted that the sedimentation rate is distinctly higher in unit B1 than that in unit A, which indicates that a greater sediment supply reached the continental slope and rise during the deglacial period than during the Holocene. Increased sedimentation rates during the deglacial period have been reported in the continental slope of the Antarctic Peninsula and Wilkes Land (Weber et al., 1994; Pudsey and Camerlenghi, 1998; Pudsey, 2000; Tooze et al., 2020). The absence of a reliable date for the bottom of unit B2 means that the sedimentation rates of the glacial period could not be calculated. Similar to the continental shelf, sediment deposition on the continental slope and rise around Antarctica has changed in response to the activity of the AIS between the glacial and interglacial periods (e.g., Anderson et al., 2014). During the glacial period, glacial tills were deposited on the edge of the continental shelf and the upper continental slope and then transferred to the lower continental slope and continental rise by turbidity currents (Larter and

Barker, 1989; Pudsey, 2000). For example, Grobe and Mackensen (1992) highlighted the importance of the melt-water beneath the ice sheet and the gravity flow from the shelf edge or upper continental slope for transporting sediments to the lower continental slope and continental rise in the Weddell Sea at the LGM. Thus, the glacial activity led to increased sedimentation in the continental slope and rise of the central Ross Sea during the glacial period, although some sediments may have been input from the bottom current as well.

The sediments of unit A commonly contained IRDs (Fig. 3). The brownish sediments in the Antarctic Ocean generally represent seasonal sea ice conditions during warm interglacial periods (Grobe and Mackensen 1992; Pudsey and Camerlenghi, 1998; Pudsey, 2000). The MS intensity is normally high for both diamicton and glacial till on the continental shelf during the glacial period (Licht et al., 1999). In contrast, during the interglacial period, the MS intensity increases with the IRD-enriched coarse-grained sediments (Licht et al., 1999; Salvi et al., 2006; Smith et al., 2019). The abundance of IRDs in the interglacial sediments is related to the presence of icebergs owing to an instability phase in the RIS system during the retreating phase. Ó Cofaigh et al. (2001) reported that IRDs peaked during the interglacial period in the Bellingshausen Sea and Weber et al. (2014) reported that the IRDs increased during the deglacial period in the Weddell Sea with an increase in the seawater temperature and a sea level rise. McGlannan et al. (2017) reported that the high IRDs occurred during the deglacial period due to the increasing icebergs by the unstable Ross Ice Sheet at the outer shelf of Wales Deep Basin in the Ross Sea, in addition to the continuous supply of the IRDs transported by the icebergs from the inner shelf. The MS intensity of unit A in the three studied cores was influenced by the number of IRDs and the sand fraction (Fig. 3). Many IRDs in unit A indicated that the deposition of sediments was influenced by an increase in the number of calving events during the warm period, although the exact age of unit A seems uncertain. Nonetheless, IRD contents in unit A decreased from Site C3 to C1, with increasing water depth and farther away from the continental shelf (Fig. 3). The IRDs originating from the continent were transported by icebergs from the calving line of the RIS to the continental shelf. Ha et al. (2018) reported that the clay mineral composition of the fine-grained

sediments in GC2. Unit A of GC2 was characterized by lower illite and higher smectite and kaolinite than unit B2. This indicates that the supply of illite by melt-water from the Ross Ice Shelf decreased whereas the supply of smectite and kaolinite increased due to the ASC that flowed westward from the Marie Byrd Land to the study area during the Holocene. Thus, the supply of unit A sediments that were transported by icebergs from the inner continental shelf and currents from the eastern side of the Ross Sea increased in the continental slope and rise to the east of Hillary Canyon, whereas the supply by melt-water or debris flow under the ice sheet or ice shelf decreased due to the retreat of the RIS on the continental shelf.

Unit B1 of GC3 and GC2 is characterized by an increasing amount of IRD upward from the lower to upper parts and fluctuations in the MS intensity with the sand fraction, suggesting that unit B1 could represent the transitional phase between the last glacial and Holocene periods. McKay et al. (2008) reported that the sandy sediments in the Ross Sea were supplied from the Transantarctic Mountains, including the McMurdo volcanic group, during the advance and retreat of the RIS. The mineral composition of the IRDs at 38 cm in unit B1 of GC3 is mainly aluminosilicates accompanied by significant amounts of hornblende and mica (Fig. 4). The hornblende may have been supplied from igneous and high-grade metamorphic rocks in the Transantarctic Mountains (Licht et al., 2005). The grayish sediments in unit B2 of GC3 and GC2 are characterized by sparse IRDs and slight fluctuations in the MS (Fig. 3). These sediments were commonly deposited in the Antarctic Ocean during the glacial period (e.g. Grobe and Mackensen, 1992; Pudsey and Camerlenghi, 1998; Pudsey, 2000; Weber et al., 2014). In addition, fewer IRDs were supplied to the formation of unit B2 in GC3 and GC2 during the glacial period because of lower iceberg formation (Smith et al., 2019). The fine-grained sediments of unit B2 in GC2 are characterized by more illite and less smectite and kaolinite than unit A (Ha et al., 2018). This indicates that during the glacial period, fine-grained sediments containing more illite may have been transported from the Antarctic continent toward the continental slope and rise to the east of Hillary Canyon by the melt-water flowed beneath the RIS that advanced to the shelf edge. This also indicates that unit B contains continental shelf sediments that were reworked

and transported by melt-water or debris flow beneath the advancing RIS. However, no significant difference of the number of IRDs and MS intensity was observed between units A and B2 of GC1 (Fig. 3). This may indicate the possibility of a different sedimentation environment on the continental rise of the central Ross Sea.

#### 4.2. Change in the geochemical and isotopic properties among lithologic units

Unit A is interpreted as interglacial sediments and shows a low degree of biogenic productivity, as denoted by the TOC, TN, and biogenic opal contents, in the continental slope and rise of the central Ross Sea, as compared to the surface sediments on the continental shelf. The low biogenic productivity in the continental slope and rise can be attributed to the decreased phytoplankton bloom during the long period of sea ice coverage on the surface water, which led to low nutrient availability (Arrigo et al., 2000; Smith et al., 2014). The surface water conditions on the Antarctic continental margin have changed from permanent multi-year ice to seasonal open marine conditions over time, depending on the sea level and seawater temperature (e.g. Grobe and Mackensen, 1992; Pudsey, 2000; Kim et al., 2020). Following the LGM, the biogenic properties increased along with the development of seasonal open marine conditions on the continental shelf (e.g. Cunningham et al., 1999; Domack et al., 1999; Salvi et al., 2006) and the continental slope of the Ross Sea (Kim et al., 2020; Khim et al., 2021; Melis et al., 2021). The distinct increase in the biogenic properties within unit A in the three cores indicates the development of seasonal open marine conditions accompanied by an increase of primary productivity in the surface water during the late Holocene.

The geochemical properties of unit B1 demonstrate the transition from glacial unit B2 to Holocene unit A (Fig. 5). Notably, the TOC, TN, and biogenic opal contents of unit B2 are higher than those of unit A, which indicates the enhanced biogenic productivity. This implies that productivity was higher during the glacial period than during the Holocene in the study area. However, this contradicts the previous results indicating that biogenic productivity was higher during the interglacial period (Brambati et al., 1997; Cunnuningham and Leventer, 1998; Salvi et al., 2006; Kim et al., 2020). The biogenic production in

the continental shelf of the Ross Sea decreased significantly during the glacial period because of the advancing RIS and the permanent sea ice. During the same period, primary production generally decreased on the continental slope and rise of the northwestern Ross Sea because of the limited light conditions (Kim et al., 2020). Thus, the higher geochemical contents in unit B, which represents a high degree of productivity, probably occurred due to alternative processes.

The TOC, TN, and biogenic opal contents of unit B2 are almost similar to those of the present-day sediments on the continental shelf (Prorathro et al., 2018). The continental shelf sediments were covered with the advancing RIS during the glacial period (Anderson et al., 2014). The increase in the sediment supply to the continental slope and rise as a result of glacier activity and the melt-water of glacial plumes is evidenced by the higher sedimentation rate in unit B. The continental shelf sediments containing high biogenic components that were deposited during the interglacial periods were found to be eroded by the advancing AIS and transported by melt-water or ice along with other terrigenous materials from the shelf edge to the continental slope and rise (Grobe and Mackensen, 1992; Weber et al., 1994; Pudsey, 2000; O'Brien et al., 2020). Thus, the glacier activity and melt-water beneath the ice sheet, which advanced to the shelf edge during the glacial period, led to the reworking and transportation of the biogenic particle-enriched shelf sediments to the continental slope and rise, resulting in the high biogenic contents of unit B2. In addition, the upward decreasing biogenic content from unit B2 to unit B1 may indicate a lower supply of shelf sediments during deglaciation because of the retreat of the RIS. Our results confirm Khim et al. (2021) who reported that the deglacial and glacial sediments in the Central Basin of the northwestern Ross Sea were characterized by higher TOC and biogenic opal contents than the Holocene sediments.

Our interpretation is also supported by correlation between the geochemical properties (Fig. 6). In general, the TOC and TN contents are linearly correlated with different slopes depending on the marine or terrestrial origin. The C/N ratio identifies the origin of organic matter, with a higher C/N ratio representing a greater contribution of terrestrial or regenerated organic matter (Meyers, 1994). The relationship between the TOC and TN contents in unit A of the cores is

different from that in units B1 and B2, except for GC1 (Fig. 6). Organic nitrogen degrades more easily than organic carbon during post-depositional oxidation of organic matter within the sediments (Kristensen and Blackburn, 1987). It implies that degraded organic matter is slightly enriched in organic carbon. Compared with unit A, the TOC contents of units B1 and B2 are enriched relative to the TN content, indicating the presence of degraded organic matter in units B1 and B2.

The positive relationship between the TOC content and C/N ratio demonstrates that the higher TOC contents and C/N ratios in units B2 and B1 could be attributed to the input of terrestrial organic matter rather than marine diatom production. The supply of large amounts of terrestrial organic matter to the study area would be difficult in a present-day scenario because of the further distance away from the coastal areas. However, during the glacial period, the advancing RIS may have transported terrestrial organic matter toward the shelf edge, which may be the reason for the prominent terrestrial influence on the continental slope and rise. However, the differential degradation between organic carbon and nitrogen during post-deposition led to an increase in the C/N ratio (Kristensen and Blackburn, 1987), resulting in its positive relationship with the TOC content. Thus, rather than glacial activity, the strong correlation between the high TOC content and C/N ratio in units B1 and B2 can be attributed to the presence of regenerated organic matter in the eroded shelf sediments, which preserved the interglacial biogenic components.

Although Site C1 in the continental rise is located farther from the shelf edge than Sites C2 and C3 (Fig. 1), the TOC (~0.6%), TN (up to 0.033%), and biogenic opal (up to 30%) contents of unit B2 in GC1 are higher than those in GC2 (~0.2%, 0.025%, and ~16%, respectively) and GC3 (~0.3%, 0.026%, and ~16%, respectively) (Fig. 5). If the sedimentation rate in unit B2 decreased as the water depth increased, the sediment supply that transported biogenic components from the shelf edge to Site C1 would be reduced, leading to the observed decrease in biogenic contents. However, the high biogenic contents of GC1 as compared to those of GC2 and GC3 might be due to some other factors. Furthermore, it is noteworthy that the relationship between the TOC and TN content is similar between units A ( $r^2 = 0.62$ ) and B2 ( $r^2 = 0.79$ ) in GC1 (Fig.

6). This implies that additional seasonal production may have occurred at Site C1 in the surface waters of the continental rise during the glacial period. Ice free areas or polynyas generally develop by either katabatic winds from the continent or the upwelling of relatively warm deep water (Martin, 2001). Grobe and Mackensen (1992) and Smith et al. (2010) suggested the possible formation of polynya in the continental rise of the Weddell Sea during glacial periods. Pudsey (2000) also reported that diatom production occurred in the polynya that developed on the continental rise of the Antarctic Peninsula during the glacial periods. The warm CDW could not intrude onto the continental shelf during glacial periods because of the advancing RIS; thus, the warmer water would have melted the ice front (e.g. Gales et al., 2021). The temporary polynya at the front of advancing ice sheet margin might have formed on the continental rise area because of the upwelling warm water. Therefore, the higher biogenic contents in unit B2 of GC1, which represents the degree of productivity, indicate that permanent sea ice did not cover the entire continental rise in the central Ross Sea during glacial periods.

The  $\text{CaCO}_3$  content in the studied cores was generally low (up to  $\sim 0.2\%$ ) in unit A, and slightly higher ( $\sim 2\%$  in GC2 and GC3 and  $\sim 0.5\%$  in GC1) in unit B (Fig. 5). Such low  $\text{CaCO}_3$  contents are common in the Holocene sediments of the Antarctic continental margin. Anderson (1975) reported that the dissolution of the  $\text{CaCO}_3$ -bearing phases during the interglacial periods in the Weddell Sea was caused by an increase in the production of corrosive dense bottom water (i.e.,  $\text{CO}_2$ -rich AABW), which intensified the dissolution of  $\text{CaCO}_3$  on the seafloor. Kim et al. (2020) reported that the continental shelf edge sediments of the Iselin Bank in the central Ross Sea contained low  $\text{CaCO}_3$  contents during interglacial periods, which is partly attributed to the increasing effect of the dense shelf water and the  $\text{CO}_2$ -enriched CDW and partly to dilution by fine siliceous detritus. Thus, the slightly high  $\text{CaCO}_3$  content during glacial periods may also be due to lower dissolution on the continental slope and rise in the central Ross Sea. During the glacial period, the polar front in the Southern Ocean migrated northward because of an increased glacial formation and lower temperatures in Antarctica (Govin et al., 2009). In addition, the effects of CDW and AABW decreased on the eastern side of Hillary Canyon, leading to the



sinking of the calcite compensation depth (Anderson et al., 1975).

The  $\delta^{13}\text{C}$  and  $\delta^{15}\text{N}$  values of sedimentary organic matter are controlled by diverse factors (summarized in Altabet, 1996). The  $\delta^{13}\text{C}$  values of organic particles mainly depend on changes in  $[\text{CO}_2]_{\text{aq}}$  and seawater temperature, the types of autotrophic species (marine or terrestrial), and/or diagenetic alteration, along with the growth rate and species diversity of phytoplankton (Rau et al., 1997). Similarly, the  $\delta^{15}\text{N}$  values of particulate organic matter are mainly influenced by the dynamics of inorganic nitrogen compounds in surface water (Altabet, 1996), and to a lesser extent, by the trophic structure of the ecosystem (DeNiro and Epstein, 1981). The  $\delta^{13}\text{C}$  and  $\delta^{15}\text{N}$  values of the deep-sea sediments have been used to trace paleobiogeochemical changes in the surface ocean that can be related to paleoproductivity and atmospheric  $p\text{CO}_2$  levels (Francois et al., 1992; Altabet et al., 1995). Despite many complicated factors along the Antarctic continental margin, the  $\delta^{13}\text{C}$  and  $\delta^{15}\text{N}$  values of organic matter are generally higher when they are assimilated during enhanced production conditions in the warm interglacial period (Rau et al., 1991; Villinski et al., 2000; Robinson and Sigman, 2008). It is interesting, within an analytical precision, that unit A is characterized by low  $\delta^{13}\text{C}$  ( $-25.2\text{‰}$ ,  $-24.8\text{‰}$ , and  $-24.7\text{‰}$  in GC3, GC2, and GC1, respectively) and high  $\delta^{15}\text{N}$  ( $4.6\text{‰}$ ,  $4.7\text{‰}$ , and  $5.5\text{‰}$  in GC3, GC2, and GC1, respectively) values whereas unit B2 is characterized by slightly high  $\delta^{13}\text{C}$  ( $-24.8\text{‰}$ ,  $-24.6\text{‰}$ , and  $-24.6\text{‰}$  in GC3, GC2, and GC1, respectively) and slightly low  $\delta^{15}\text{N}$  ( $3.8\text{‰}$ ,  $4.0\text{‰}$ , and  $4.9\text{‰}$  in GC3, GC2, and GC1, respectively) values with transitional values in unit B1 (Fig. 5). However, these isotope results seem unlikely to vary depending on the interglacial and glacial conditions. The  $\delta^{13}\text{C}$  and  $\delta^{15}\text{N}$  values of unit A are assumed to represent the seasonal production of *in situ* organic particles during the warm interglacial periods. The slightly higher  $\delta^{13}\text{C}$  values of units B1 (deglacial) and B2 (glacial), as compared to those of unit A, are not a result of enhanced production as in the case of biogenic TOC and TN. Such a slight increase in the  $\delta^{13}\text{C}$  values of units B1 and B2 may be attributed to the incorporation of regenerated organic matter from the shelf sediments that were subject to selective diagenesis and/or a greater contribution of organic matter that originated from sea ice. The slightly low  $\delta^{15}\text{N}$  values of units B1 and B2 also support the theory of limited production

during cold glacial periods, together with a relatively higher contribution of sea ice-originated organic matter (Cozzi and Cantoni, 2011). Although units A and B might be distinguished by their  $\delta^{13}\text{C}$  and  $\delta^{15}\text{N}$  values with respect to *in situ* surface water productivity, more precise examination and robust interpretation are required due to the complicated factors responsible for their values in the Antarctic organic particles.

#### 4.3. Paleoenvironmental reconstruction in the continental slope and rise of the central Ross Sea

Figure 7 depicts the schematic paleoenvironmental model in terms of glaciomarine sedimentation in the continental slope and rise to the east of Hillary Canyon in the central Ross Sea. The Antarctic environment is strongly affected by the advance and retreat of the ice sheet, which interacts with the developing ice shelf and seasonal sea ice (Anderson et al., 1980; Grobe and Mackensen 1992; Domack et al., 1999; Pudsey 2000; Gales et al., 2021). During the glacial period, the grounding line of the advancing RIS was located near the shelf edge on the east of the Pennell Bank and the sea ice coverage extended toward the continental slope and rise (Shipp et al., 1999; Halberstadt et al., 2016; Bart et al., 2018; Anderson et al., 2019). During this time, the pressure of the advancing RIS led to extensive erosion on the continental shelf, resulting in the deposition of diamicton (Anderson et al., 1984; Domack et al., 1999). Unit B2 in the study area represents the glacial sediments, with permanent sea ice covering the continental slope and rise on the east of Hillary Canyon. Thus, the unsorted sediments of unit B2 were mainly supplied from the continental shelf by melt-water or debris flow by the erosion of the advancing RIS to the continental slope and rise (Fig. 7a). The degree of sediment transport decreased further from the continental shelf, where the sediments were eroded and reworked. Consequently, the sedimentation rate of unit B2 decreased from GC3 to GC1 (Fig. 3). Reduced primary productivity (in terms of biogenic content) was observed in the continental slope and rise of the central Ross Sea, compared with that during the interglacial periods. Glacial productivity was also very low on the continental slope and rise of the western Ross Sea (Ceccaroni et al., 1998; Kim et al., 2020), Antarctic Peninsula (Pudsey, 2000), and Weddell

Sea (Grobe and Mackensen, 1992). Based on TOC and biogenic opal contents, GC1 located in the lower continental rise recorded seasonal sea ice coverage or occurrence of limited polynya, that supplied *in situ* biogenic sediments. The low smectite content of unit B2 in GC2 indicates that the clockwise surface current in the continental shelf was blocked by the advancing RIS (Ha et al., 2018). In addition, because of the advancing RIS on the eastern continental shelf, the production of corrosive AABW was restricted, resulting in slightly better preservation of CaCO<sub>3</sub> in the study area.

After the LGM, the RIS began to retreat rapidly on the continental shelf of the eastern Ross Sea (Mosola and Anderson, 2006; Bart et al., 2018). During the deglacial period, the depositional process depended on the distance from the grounding line of the retreating ice sheet and ice shelf (Domack et al., 1999; Smith et al., 2019). A grounding zone wedge formed at the front of the grounding line, fine-grained sediments were deposited beneath the ice shelf, and biogenic particles sunk under the seasonal open marine conditions that occurred on the continental shelf of the western Ross Sea (Domack et al., 1999). The permanent sea ice developed a multi-year or seasonal sea ice coverage on the continental slope and rise of the Weddell Sea and the Antarctic Peninsula during this period (Grobe and Mackesen 1992; Pudsey, 2000). Similarly, the sea ice on the continental slope and rise of the central Ross Sea, which resulted in a gradual increase in biological production, might have attained multi-year or seasonal coverage (Fig. 7b). The effect of the RIS on the continental slope and rise was significantly reduced, and the supply of sediments from the continental shelf by melt-water or debris flow also diminished. The sediment properties of unit B1 changed gradually from unit B2 (glacial) to unit A (Holocene). An increase in the IRDs in unit B1 reflects the seawater temperature rise, the collapse of the retreating ice shelf, and the production of icebergs during deglaciation (Barker et al., 1999; Salvi et al., 2006).

During the Holocene, the environment in the continental margin of the Ross Sea is characterized by seasonal open marine conditions, with the biological productivity of the surface water being enhanced in spring and summer (Prothro et al., 2018; Khim et al., 2021; Torricella et al., 2021). However, biological productivity mainly occurs in the southern and western parts of the

continental shelf in the Ross Sea (Arrigo et al., 2000; Arrigo and van Dijken, 2004). The surface sediments in the Ross Sea are characterized by abundant biogenic particles in deep basins and troughs, remnant sediments that have been winnowed by the bottom currents on shallower banks, and IRDs transported by icebergs from the calving line (McGlannan et al., 2017; Prothro et al., 2020; Hartman et al., 2021). The higher percentage of gravel and sand in unit A is related to the increasing supply of IRDs by icebergs due to the increase in seawater temperature and the sea level rise. The increase in the biogenic contents within unit A, represented as surface water productivity, indicates the enhanced biological productivity during the late Holocene (Fig. 7c). The high smectite content of unit A reflects that the surface current in the continental shelf of the Ross Sea flows clockwise from Victoria Land toward the continental slope (Ha et al., 2018). With the complete retreat of the RIS, nutrient-enriched CDW has intruded the inner continental shelf and corrosive AABW is actively produced in the inner shelf and flows toward the continental slope and rise (Jacobs, 2004), where it results in the poor preservation of  $\text{CaCO}_3$  within the sediments.

## 5. Conclusions

To comprehend the changes in glaciomarine sedimentation on the continental slope and continental rise of the central Ross Sea since the LGM, box and gravity cores were obtained at three sites (C1, C2, and C3), on the eastern side of Hillary Canyon. The sedimentological, geochemical, and isotopic properties of the core sediments were analyzed along with AMS  $^{14}\text{C}$  dating of the bulk sediments. A comparison of the box cores with the tops of the gravity cores demonstrated the minimal core-top loss of the gravity cores and the favorable preservation of the Holocene record. The core-top sediments yielded relatively old AMS  $^{14}\text{C}$  ages (2.5 ka, 5.7 ka, and 1.5 ka in GC1, GC2, and GC3, respectively), because of the old carbon in the seawater around the Antarctic continental margin. Based on the analytical results and preliminary descriptive data, the lithologic facies were divided into two units (A and B), and unit B was subdivided into two subunits (B1 and B2), related to the Holocene,

deglacial, and glacial periods. The sedimentation rates estimated by the AMS  $^{14}\text{C}$  ages decreased as the water depth increased, but were higher in the glacial period than in the interglacial period.

Unit B2, interpreted as a sedimentary stratum laid during the glacial period, shows relatively low  $\delta^{15}\text{N}$  and TN with high biogenic opal, TOC,  $\delta^{13}\text{C}$ , C/N ratio, and  $\text{CaCO}_3$  content. The sediments of unit B2 were transported from the continental shelf by melt-water under the ice sheet or from the distal part of the debris flow in front of the grounding line of the continental shelf. Based on the expected sedimentation rate for unit B2, the degree of sediment transport from the shelf area seems to decrease as the water depth increases. Unit B1 may correspond to the sediments deposited during the transition period from the glacial to interglacial periods. In this unit, the biogenic opal, TOC,  $\delta^{13}\text{C}$ , C/N ratio, and  $\text{CaCO}_3$  content decrease, while  $\delta^{15}\text{N}$  and TN gradually increased upward. The geochemical signatures of unit B1 indicate that glacial sediment supply was progressively reduced, accompanied by a gradual increase in the biogenic productivity of the surface water. Unit A, interpreted as the sediments deposited during the Holocene, shows relatively low biogenic opal, TOC,  $\delta^{13}\text{C}$ , C/N ratio, and  $\text{CaCO}_3$  with high  $\delta^{15}\text{N}$  and TN. The biogenic components of unit A were mainly supplied by the biogenic productivity in surface water under seasonal sea ice conditions, but the degree of productivity was lower than the continental shelf. The biogenic opal and TOC contents during the glacial period at Site C1 in the continental rise reflect seasonal sea ice conditions; however, Sites C2 and C3 were covered with permanent sea ice.

Similar to the continental shelf of the Antarctic continental margin, sedimentation on the continental slope and rise of the central Ross Sea was largely affected by the advance and retreat of the RIS. Due to the advancing RIS toward the shelf edge during the glacial period, more sediments were transported from the continental shelf to the continental slope and rise by melt-water under the ice sheet or the debris flow at the front of the grounding line. During the transition period, the effect of the ice sheet was gradually reduced because of the retreat of the RIS and more biogenic sediments were supplied from the surface water. The downward settling of the biogenic particles generated by the enhanced biogenic productivity in the surface water during the

interglacial period was the main source of biogenic components of sediments in the continental slope and rise on the east of Hillary Canyon in the central Ross Sea.



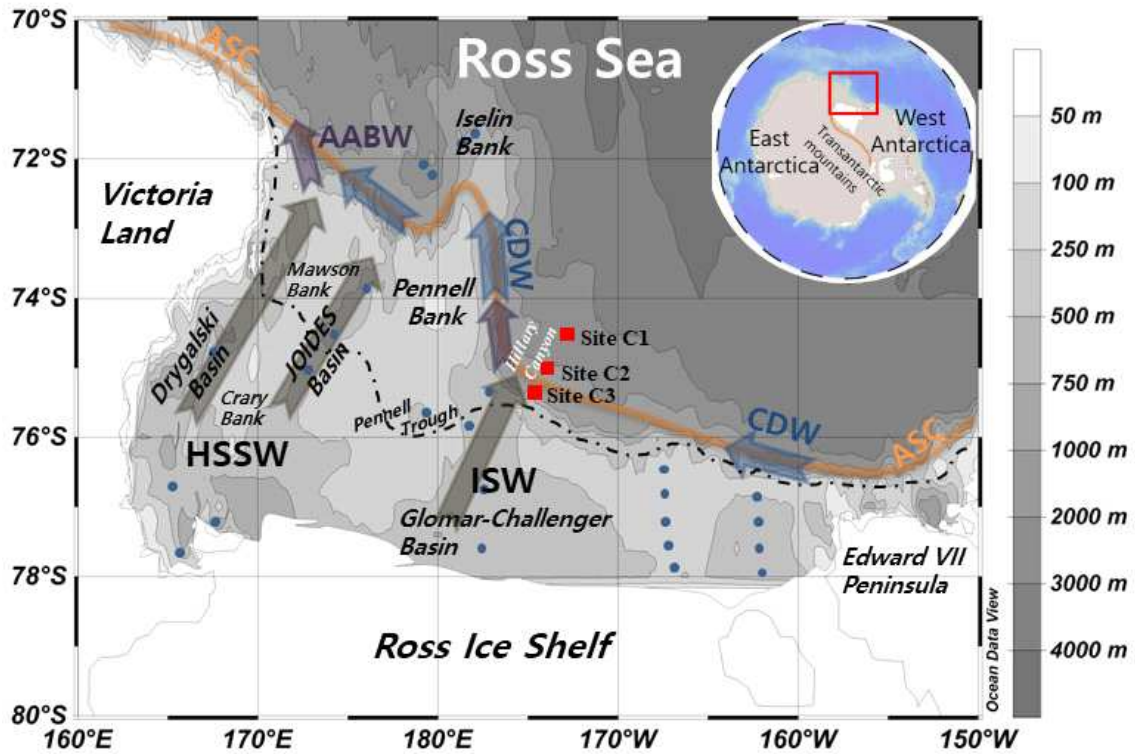


Figure 1. Map of the study area showing the locations of the coring sites. Three gravity (GC3, GC2, and GC1) and box (BC3, BC2, and BC1) cores were obtained, respectively, at the three sites (RS14-C3, C2, and C1) in the continental slope and rise to the east of Hillary Canyon in the central Ross Sea. The solid-dotted line represents the limit of the RIS advance during the LGM (after Anderson et al., 2019). ASC: Antarctic Slope Current, AABW: Antarctic Bottom Water, CDW: Circumpolar Deep Water, HSSW: High Salinity Shelf Water, ISW: Ice Shelf Water (Smith et al., 2014). Blue dots are coring sites of previous studies.

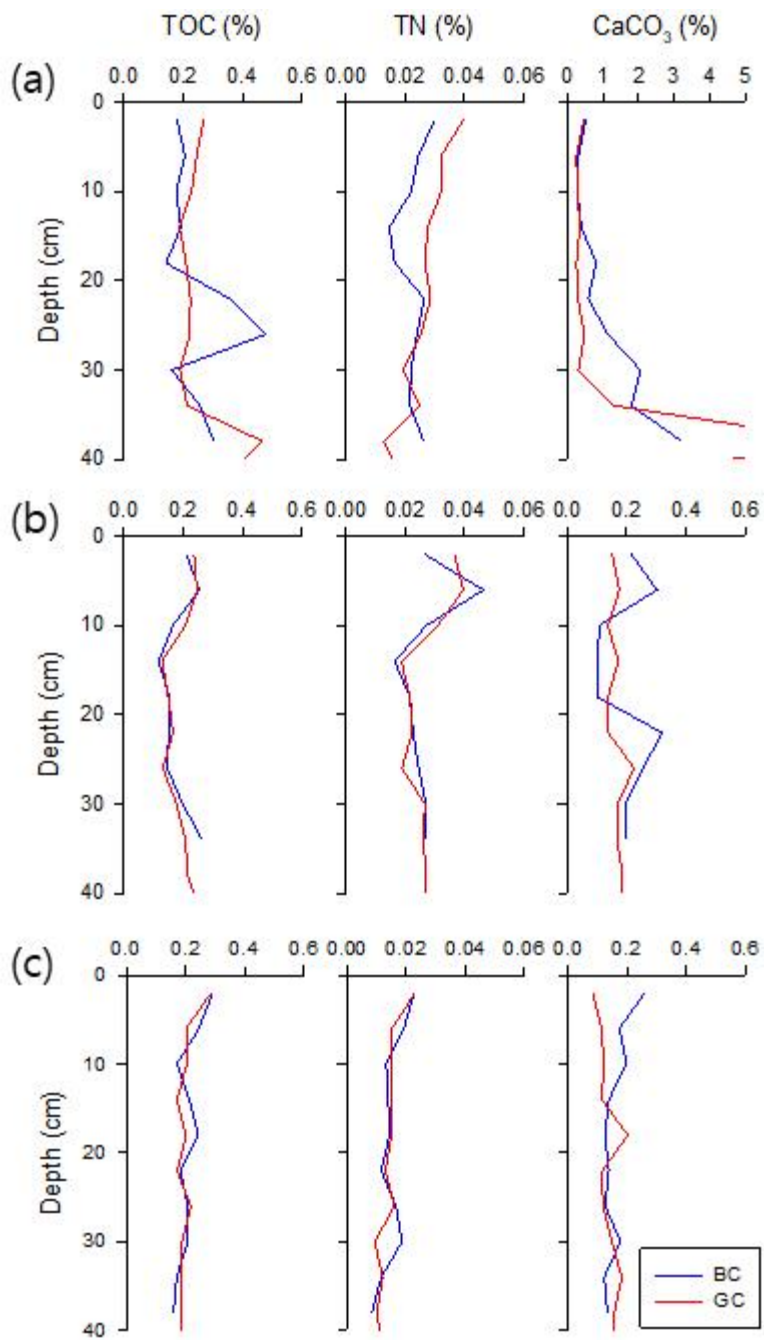


Figure 2. Comparison of geochemical properties (TOC, TN, and CaCO<sub>3</sub>) between the box cores (BC) and the upper part of the gravity cores (GC), confirming the minor loss of core-top in the gravity core. (a) Site C3, (b) Site C2, (c) Site C1.



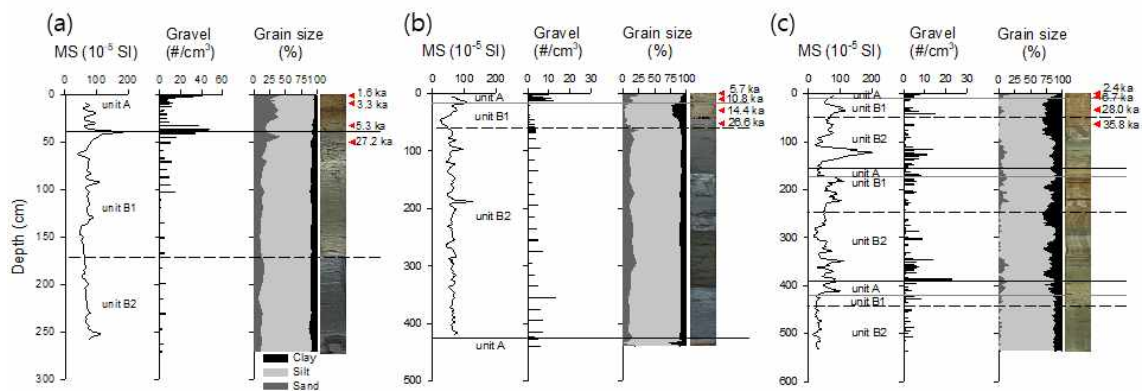


Figure 3. Downcore variation of sediment properties (magnetic susceptibility (MS), number of gravel-sized particles, and grain size). (a) GC3, (b) GC2, (c) GC1. Lithologic units (A, B1, and B2) are divided by solid and dotted lines and AMS  $^{14}\text{C}$  ages are also shown.



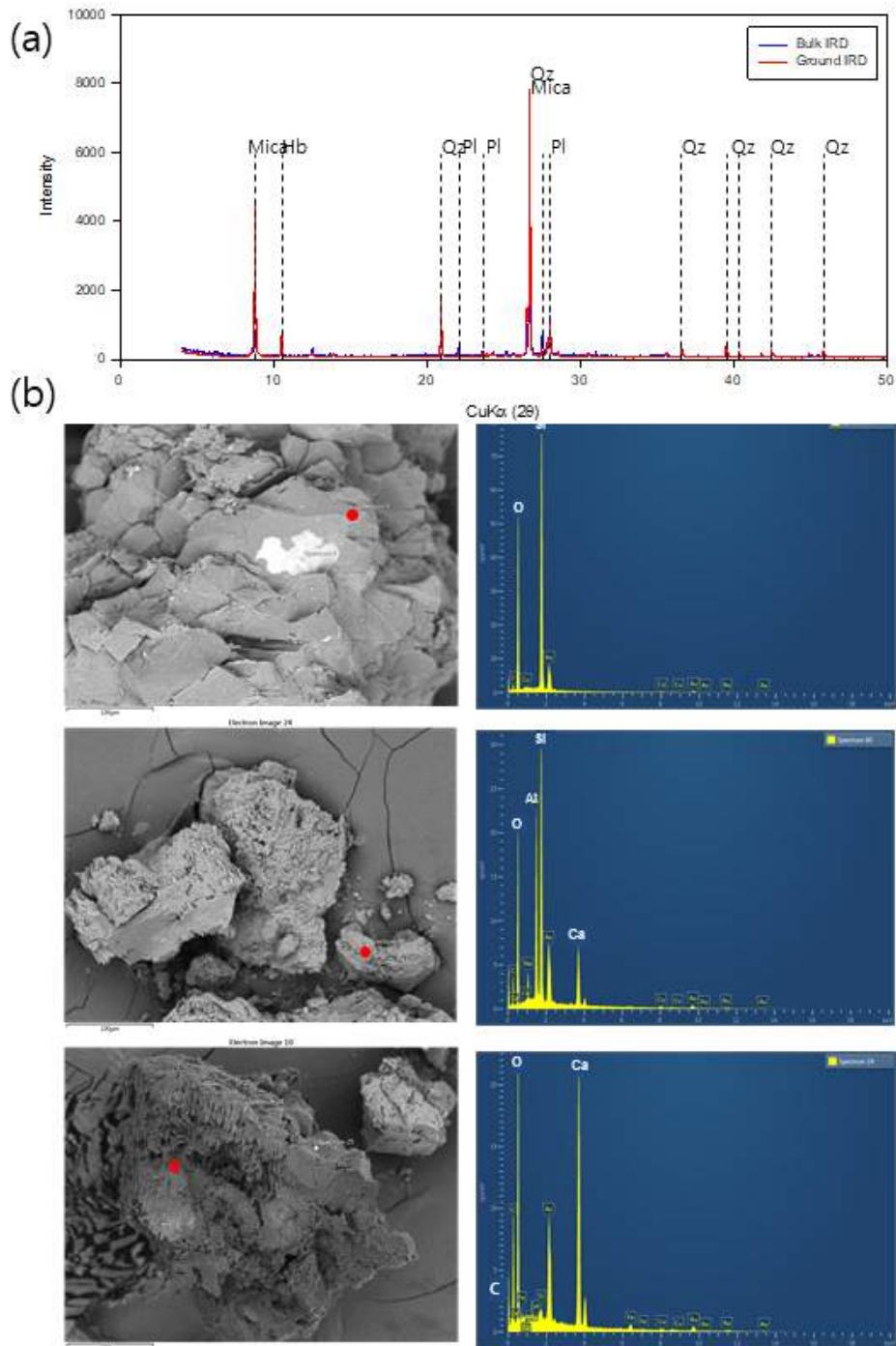


Figure 4. (a) XRD results for the mineral composition of IRD (bulk and ground) at 38 cm of GC3. Distinct peaks of hornblende and mica are clearly observed. Hb: hornblende, Qz: quartz, Pl: plagioclase. (b) SEM-EDS photos of IRDs at 38 cm of GC3. The dominant minerals are aluminosilicates including quartz. A Ca peak was observed in some grains.

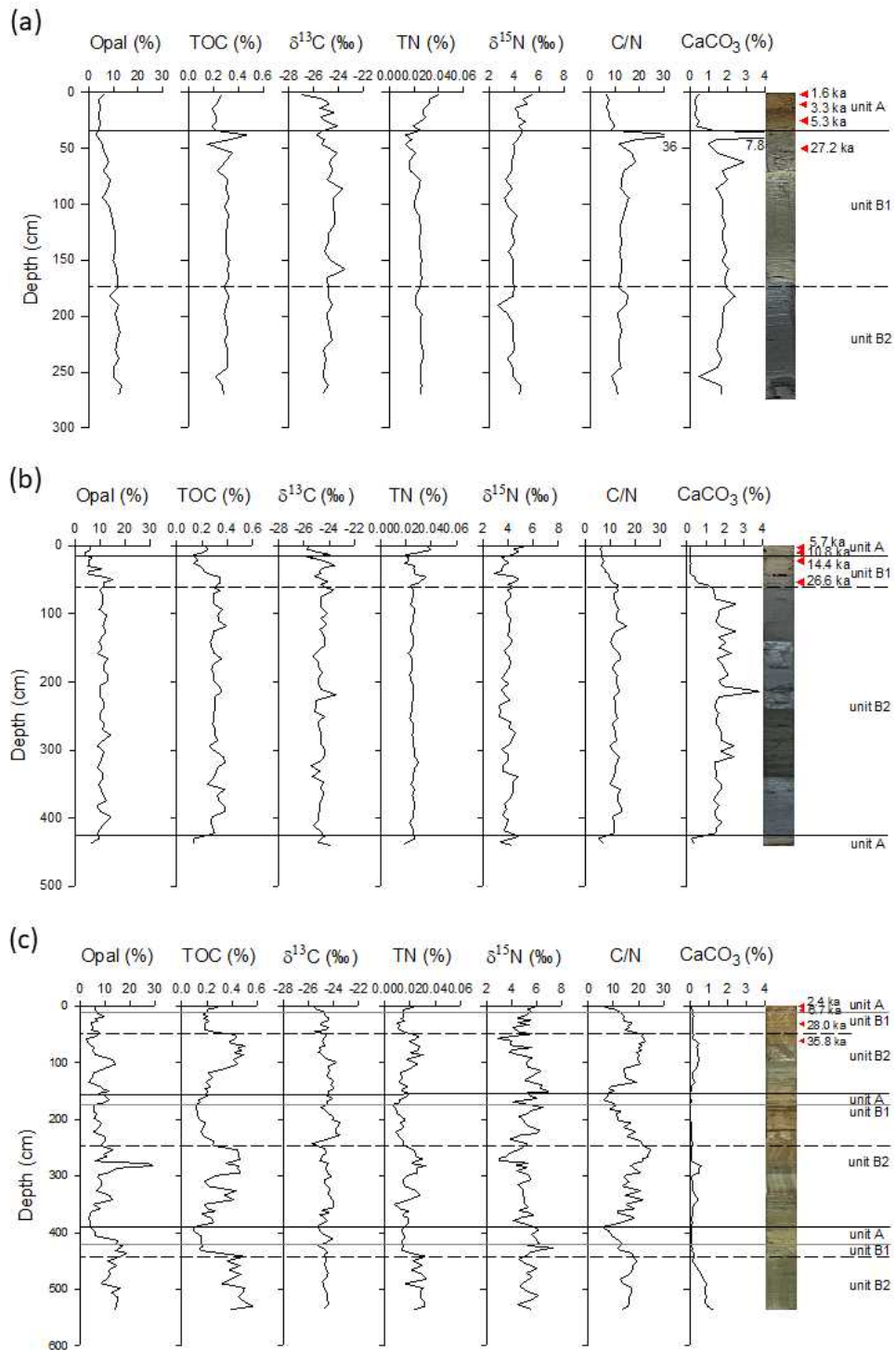


Figure 5. Downcore variation of geochemical (biogenic opal, TOC, TN, C/N, and  $\text{CaCO}_3$ ) and isotopic ( $\delta^{13}\text{C}$  and  $\delta^{15}\text{N}$ ) properties. (a) GC3, (b) GC2, (c) GC1. Lithologic units (A, B1, and B2) are divided by solid and dotted lines and AMS  $^{14}\text{C}$  ages are also shown.

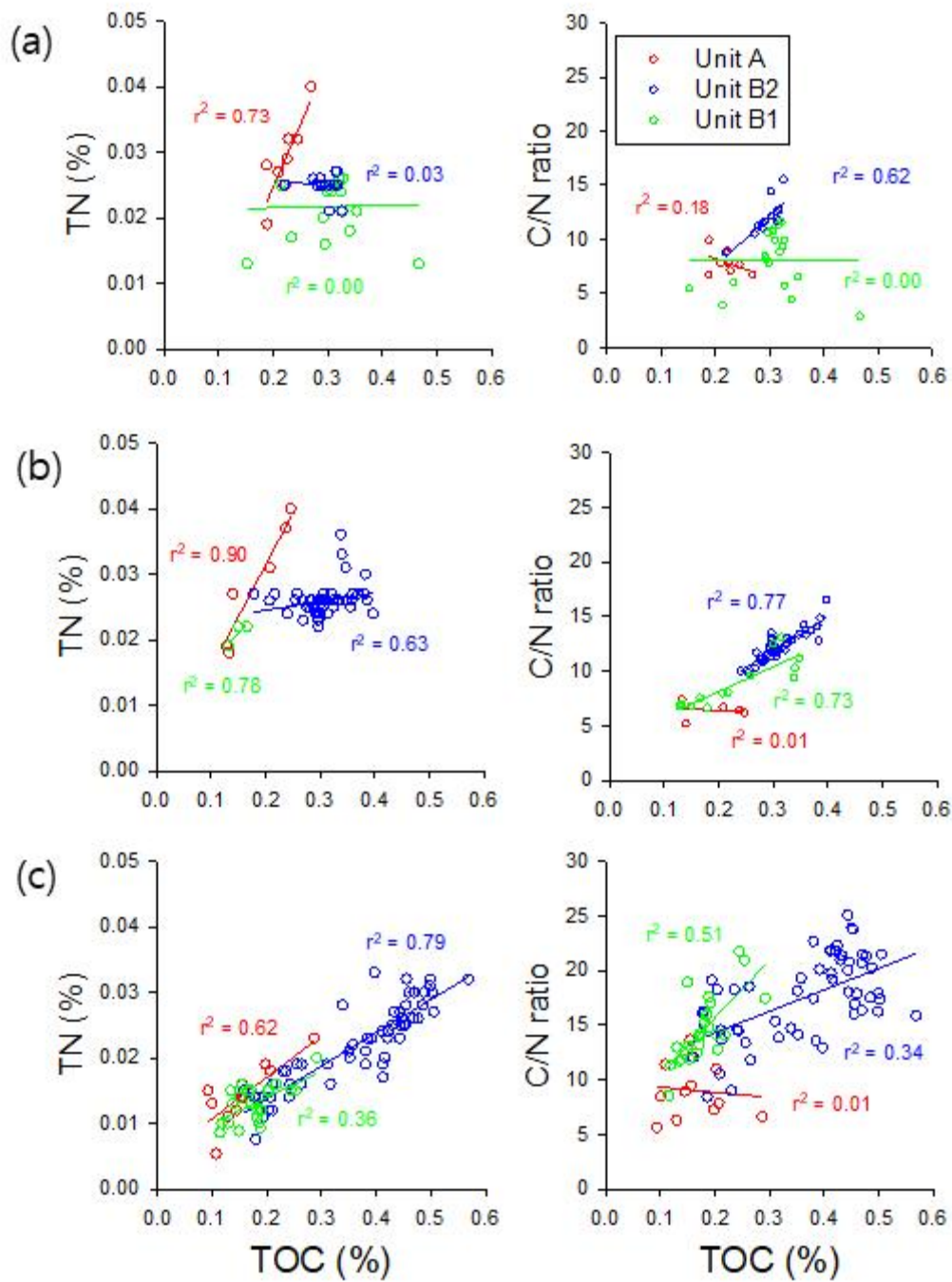


Figure 6. Correlations between TOC and TN contents and between TOC content and C/N ratio. (a) GC3, (b) GC2, (c) GC1.

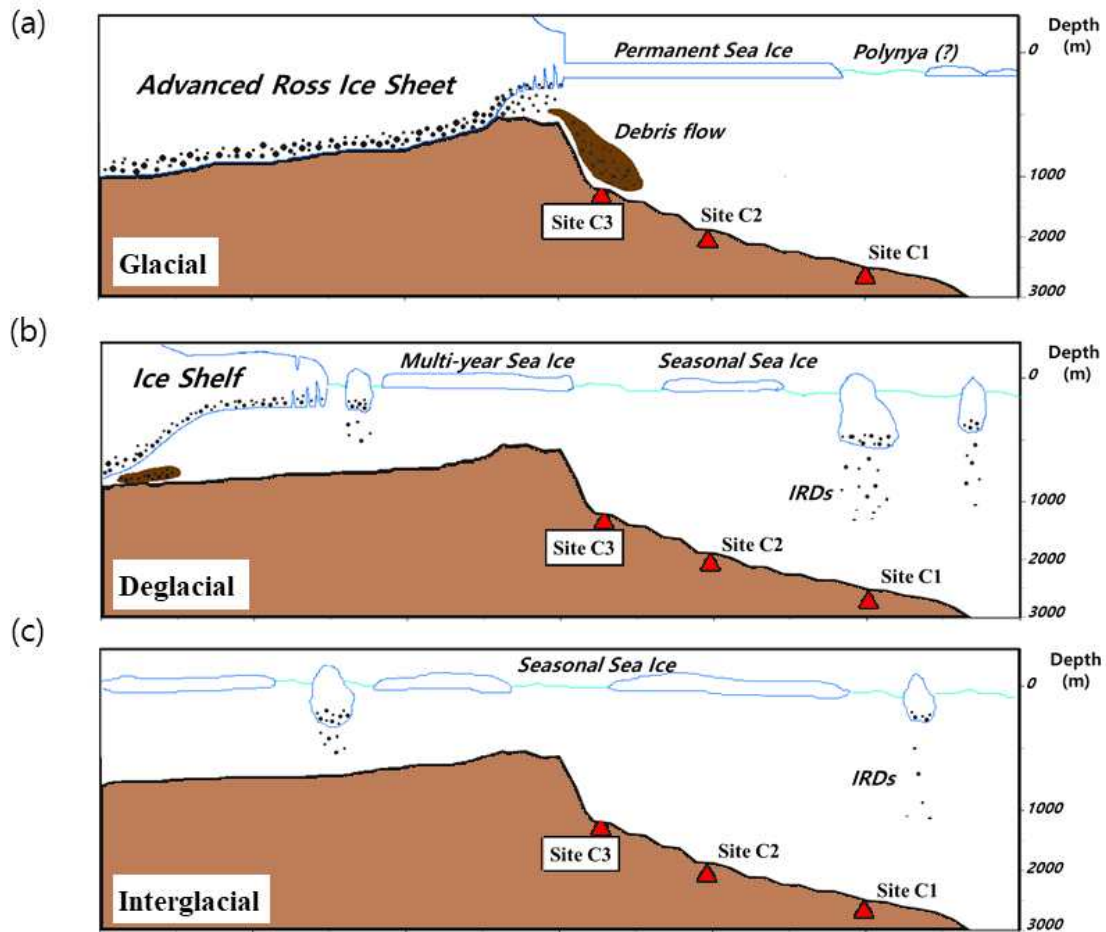


Figure 7. Schematic model of paleoenvironmental condition showing the activity of the RIS and glaciomarine sedimentation on the continental slope and rise of the central Ross Sea. (a) glacial period, (b) deglacial period, and (c) interglacial period.

Table 1. Locations of the three sites (RS14-C1, RS14-C2, and RS14-C3) in the study area.

Label	Latitude (S)	Longitude (W)	Depth (m)
RS14-C1	74°30.54'	172°51.16'	2372
RS14-C2	75°00.04'	173°55.16'	1757
RS14-C3	75°20.41'	174°36.47'	1215



Table 2. AMS  $^{14}\text{C}$  ages of box and gravity cores.

Core	Depth (cm)	Conventional $^{14}\text{C}$ ages (yr BP)	Error	LCO	LCO-corrected ages (yr BP)	$\Delta\text{R}$	Calibrated $^{14}\text{C}$ ages (yr BP)	Laboratory code
BC1	0-1	5106	34	4006	1100	1100	0	Poz-79258
GC1	0-1	7533	38	4006	3527	1100	2442	Poz-69628
	4-5	11040	57	4006	7034	1100	6701	Poz-79257
	8-9	19319	286	4006	15313	1100	17095	AWI-4811.1.2
	26-27	29074	299	4006	25068	1100	28040	Poz-69629
	52-53	36913	715	4006	32907	1100	35837	Poz-69630
BC2	0-1	4275	34	3175	1100	1100	0	Poz-79261
GC2	0-1	9317	48	3175	6142	1100	5724	Poz-69631
	6-7	13801	67	3175	10626	1100	10787	Poz-79266
	16-17	16649	140	3175	13484	1100	14448	Poz-79267
	48-49	26636	243	3175	23461	1100	26580	Poz-82577
BC3	0-1	3448	32	2348	1100	1100	0	Poz-79268
GC3	0-1	5133	38	2348	2785	1100	1568	Poz-69632
	12-13	6281	36	2348	3933	1100	3287	Poz-79272
	24-25	8135	44	2348	5787	1100	5281	Poz-82578
	50-51	26570	241	2348	24222	1100	27210	Poz-82580

극지연구소

## 제 4 장 연구개발목표 달성도 및 대외기여도

지난 3년 간의 과제 수행동안 국제학술지 5편과 국내외 학술대회에 아래와 같이 많은 발표 성과를 내어 연구 목표의 달성도는 100%를 넘는 성공적인 결과를 거두었다.

### [국제학술지 논문]

- Lee, J., Kim, S., Lee, J.I., Cho, H.G., Phillips, S.C., **Khim, B.K.\*** (2020) Monsoon-influenced variation of clay mineral compositions and detrital Nd-Sr isotopes in the western Andaman Sea (IODP Site U1447) since the late Miocene. *Palaeogeography Palaeoclimatology Palaeoecology*, vol. 538, Article 109339, (\*corresponding author)
- Lee, J., Kim, S., **Khim, B.K.\*** (2020) A paleoproductivity shift in the northwestern Bay of Bengal (IODP Site U1445) across the Mid-Pleistocene transition in response to weakening of the Indian summer monsoon. *Palaeogeography Palaeoclimatology Palaeoecology*, vol. 560, Article 110018. (\*corresponding author) (<https://doi.org/10.1016/j.palaeo.2020.110018>)
- Melis, R., Capotondi, L., Torricella, F., Ferretti, P., Geniram, A., Hong, J.K., Kuhn, G., Khim, B.K., Kim, S., Malinverno, E., Yoo, K.C., Colizza, E. (2021) Last Glacial Maximum to Holocene paleoceanography of the northwestern Ross Sea inferred from sediment core geochemistry and micropaleontology at Hallett Ridge. *Journal of Micropaleontology*, vol. 40, p.15-35.
- Khim, B.K.\*, Colizza, E., Lee, J.I., Giglio, F., Ha, S., Bak, Y.S. (2021) Biological productivity and glaciomarine sedimentation in the Central Basin of the northwestern Ross Sea. *Polar Science*, vol. 28, Article 100682. (\*corresponding author)
- Ha, S., Colizza, E., Torricella, F., Langone, L., Giglio, F., Kuhn, G., Marci, P., Khim, B.K.\* (2022) Glaciomarine sediment deposition on the continental slope and rise of the central Ross Sea since the Last Glacial Maximum. *Marine Geology*, vol. 445, Article 106752. (\*corresponding author)

### [국제학술회의 발표]

- Khim, B.K.**, Sohn, Y.K., Lee, M.K., Lee, J.I., Yoo, K.C. (2020) Laminated sediments in core RS15-LC42 in the Central Basin of the northwestern Ross Sea: preliminary microscopic results. *SCAR2020 Open Science Conference*, Hobart, Australia (Aug. 3-7)



- Ha, S., **Khim, B.K.**, Lee, J.I., Yoo, K.C. (2020) Holocene sediment deposition in the Drygalski Basin of the western Ross Sea. *SCAR2020 Open Science Conference*, Hobart, Australia (Aug. 3-7)
- Torricella, F., Capotondi, L., Caricchi, C., Del Carlo, P., Geniram, A., Giglio, F., Melis, R., Yoo, K.C., **Khim, B.K.**, Colizza, E. (2020) Oceanic versus bottom water dynamics in the Central Basin, Western Ross Sea (Antarctica), since the Last Glacial Maximum. *SCAR2020 Open Science Conference*, Hobart, Australia (Aug. 3-7)
- Melis, R., Capotondi, L., Ferretti, P., Geniram, A., Torricella, F., Di Roberto, A., **Khim, B.K.**, Colizza, E. (2020) Deglacial dynamics in the Ross Sea (Antarctica) revealed by the occurrence of the planktic foraminifer *Neogloboquadrina pachyderma*. *SCAR2020 Open Science Conference*, Hobart, Australia (Aug. 3-7)
- Torricella, F., Melis, R., Capotondi, L., Del Carlo, P., Kuhn, G., Geniram, A., Giglio, F., Yoo, K.C., **Khim, B.K.**, Colizza, E. (2020) Deglacial-Holocene environmental evolution from a multidisciplinary study on the Central Basin, Western Ross Sea. *GSA 2020 Connects Online* (Oct. 26-30), Paper No. 242-9
- Ha, S., **Khim, B.K.**, Lee, J.I., Yoo, K.C. (2021) Depositional processes in the Drygalski Basin of the Ross Sea since the Last Glacial Maximum. *The 25th International Symposium on Polar Sciences (ISPS)*, Incheon, Korea (Sept. 27-29), (S6-6).
- Geniram A., Colizza E., De Santis L., Giglio F., **Khim B.K.**, Bergamasco A., Gales J., Torricella F. (2021) Multidisciplinary analysis of three box cores collected east to the Hillary Canyon (Eastern Ross Sea, Antarctica). *The 25th International Symposium on Polar Sciences (ISPS)*, Incheon, Korea (Sept. 27-29), (S6-5)
- Colizza E., Geniram A., Giglio F., Ha S., **Khim B.K.**, Kuhn G., Macri P., Torricella F. (2021) Past and recent sedimentary dynamics recorded in sedimentary cores collected east to the Iselin Bank (Ross Sea, Antarctica). *The 25th International Symposium on Polar Sciences (ISPS)*, Incheon, Korea (Sept. 27-29), (S6-4)
- Torricella F., Colizza E., Capotondi L., Geniram A., Giglio F., **Khim B.K.**, Kuhn G., Yoo K.C., Macri P., Melis R., Sagnotti L. (2021) Pre-LGM sedimentological feature and paleo-oceanographic changes in the Central Basin (western Ross Sea). *The 25th International Symposium on Polar Sciences (ISPS)*, Incheon, Korea (Sept. 27-29), (S6-3)

- Lee, M.K., Kim, S., Bollen, M., Seong, Y.B., **Khim, B.K.**, Jang, K., Lee, J.I., Yoo, K.C., Moon, H.S., Yoon, H.I. (2021) Reconstruction of cryospheric and paleoceanographic changes of the past 1 Myrs from the record at the continental margin, NW Ross Sea. *The 25th International Symposium on Polar Sciences (ISPS)*, Incheon, Korea (Sept. 27-29), (S6-2)
- Khim, B.K.**, Lee, M.K., Sohn, Y.K., Lee, J.I., Kim, S., Yoo, K.C. (2021) Microstructure of lamination in core RS15-LC42 in the Central Basin of the northwestern Ross Sea: preliminary results. *The 25th International Symposium on Polar Sciences (ISPS)*, Incheon, Korea (Sept. 27-29), (S6-1)
- Ha, S., Colizza, E., Torricella, F., Langone, L., Giglio, F., Kuhn, G., Marci, P., **Khim, B.K.** (2022) Glaciomarine sediment deposition in the continental slope and rise of the central Ross Sea since the Last Glacial Maximum. *Ocean Science Meeting 2022*, Honolulu, USA (Feb. 27 – Mar. 4), (online)

[국내학술회의 발표]

- 하상범, 이재일, **김부근**, 유규철 (2020) 로스해 드라이갈스키 분지의 홀로세 고해양 변화. *한국해양학회 2020 추계학술발표대회 요약집*, 경주, p.GO-06.
- Yoo, K.C., Lee, J.I., Lee, M.K., Kim, S., Subt, C., Rosenheim, B., Jung, J.W., Wellner, J., Rhee, H., Kim, J., Seung, Y.B., Leventer, A., Moon, H.S., **Khim, B.K.** (2021) Features of snowball earth (the crysogenian) reincarnated in the Holocene sediments beneath the Larsen C Ice Shelf. *한국해양학회 2021 추계학술발표대회 요약집*, 제주, [SI06]
- 김부근**, 이민경, 손영관, 김성한, 이종석 (2021) 로스해 중앙분지 퇴적물 층리의 미세구조. *한국해양학회 2021 추계학술발표대회 요약집*, 제주, [SI04]
- 하상범, 이재일, 조현구, 박영숙, 유규철, **김부근** (2021) 로스해 드라이갈스키 분지 코아퇴적물의 고해양 변화 기록. *한국해양학회 2021 추계학술발표대회 요약집*, 제주, [SI03]
- 하상범, 이재일, 유규철, **김부근** (2022) 남극 로스해 드라이갈스키 분지에서 마지막 빙하기 이후 퇴적물 기원지 변화. *한국해양학회 2022 추계학술발표대회 요약집*, 강릉, [GO12]

## 제 5 장 연구개발결과의 활용계획

Our contemporary understanding of the state of the West Antarctic ice sheet is often traced to the prescience of Mercer, who 40 years ago suggested that anthropogenic climate warming would destabilize ice shelves, leading to ice sheet collapse. Recent observations certainly support Mercer's understanding of the crucial role of ice shelves. Yet a solicitation of researchers' views conducted as recently as 2013 concluded that expert opinion is both "uncertain and undecided" on whether recent trends in Antarctic ice sheet behavior are owing to natural variability, or are a response to climate change. The reason for this ambiguity is simple: the record of direct observations of Antarctic ice sheet change is insufficient in length. The earliest application of satellite radar interferometry to obtain flow velocities for the Antarctic ice sheet was in 1993, and most other observational products, such as the satellite altimetry critical for evaluating thinning rates, are even more recent. Modern geophysical observations of the ice sheet thus comprise a period less than the standard textbook requirement for a representative climatology - 30 years - against which trends can be evaluated. This is surely too short a time to have observed the Antarctic ice sheet, characterized by intrinsic variability on even longer timescales than the atmosphere, and expect a definitive answer. Unless we are willing to wait another few decades or more - by which time the answer may well be clear, but no longer as useful - we need to incorporate information from paleoclimatology.

## 제 6 장 참고문헌

### 1 절. Recycled biogenic components of the Pleistocene glaciomarine laminated muds in the Central Basin of the northwestern Ross Sea and their paleoclimatic implications

- Anadon R, Estrada M (2002) The FRUELA cruises. A carbon flux study in productive areas of the Antarctic Peninsula (December 1995–February 1996). *Deep-sea Research. Part II*, 49: 567–583.
- Albot, O.B., 2016. Pleistocene cyclostratigraphy on the continental rise and abyssal plain of the western Ross Sea, Antarctica. MS Thesis, Victoria Univ. Wellington, New Zealand, 171 pp.
- Alley, K., Patacca, K., Pike, J., Dunbar, R., Leventer, A., 2018. Iceberg Alley, East Antarctic Margin: Continuously laminated diatomaceous sediments from the late Holocene. *Mar. Micropal.* 140, 56–68.
- Anderson, J.B., 1999. *Antarctic Marine Geology*: Cambridge (UK), Cambridge Univ. Press, 289 pp.
- Anderson, J.B., Conway, H., Bart, P.J., Witus, A.E., Greenwood, S.L., McKay, R.B., Hall, B.L., Ackert, R.P., Licht, K., Jakobsson, M., Stone, J.O., 2014. Ross Sea paleo-ice sheet drainage and deglacial history during and since the LGM. *Quat. Sci. Rev.* 100, 31–54.
- Bollen, M., 2019. The response of marine diatoms to environmental drivers in the Ross Sea, and applications as a paleoceanographic proxy. MS Thesis, Univ. Otago, New Zealand, 61 pp.
- Bonn, W.J., Gingele, F.X., Grobe, H., Mackensen, A., Fütterer, D.K., 1998. Palaeoproductivity at the Antarctic continental margin: opal and barium records for the last 400 ka. *Palaeogeogr. Palaeoclimat. Palaeoecol.* 129, 195–211.
- Cofaigh, C.O., Dowdeswell, J.A., 2001. Laminated sediments in glaciomarine environments: diagnostic criteria for their interpretation. *Quat. Sci. Rev.* 20,

1411–1436.

- Colleoni, F., De Santis, L., Siddoway, C.S., Bergamasco, A., Golledge, N.R., Lohmann, G., Passchier, S., and Siegert, M.J., 2018. Spatio-temporal variability of processes across Antarctic ice-bed-ocean interfaces. *Nature Comm* 9, 2289, DOI:10.1038/s41467-018-04583-0
- Domack, E.W., 1990. Laminated terrigenous sediments from the Antarctic Peninsula: the role of subglacial and marine processes. In: Dowdeswell, J.A., Scourse, J.D. (Eds.), *Glaciomarine Environments: Processes and Sediments*. Geol. Soc. London, Spec. Pub. 53, pp. 91–103.
- Domack, E.W., Powell, R., 2018. Chapter 7 – Modern glaciomarine environments and sediments: An Antarctic perspective. In: Menzies, J., van der Meer, J. (Eds.), *Past Glacial Environments*. Elsevier, pp. 181–272.
- Frignani, M., Giglio, F., Langone, L., Ravaioli, M., Mangini, A. 1998, Late Pleistocene–Holocene sedimentary fluxes of organic carbon and biogenic silica in the northwestern Ross Sea, Antarctica. *Annals Glaciol.* 27, 697–703.
- Ha, S., Colizza, E., Torricella, F., Langone, L., Giglio, F., Kuhn, G., Macrí, P., Khim, B.K., 2022. Glaciomarine sediment deposition on the continental slope and rise of the central Ross Sea since the Last Glacial Maximum. *Mar. Geol.* 445, Article 106752.
- Hall, B.L., Denton, G.H., Stone, J.O., Conway, H., 2013. History of the grounded ice sheet in the Ross Sea sector of Antarctica during the Last Glacial Maximum and the last termination. In: Hambrey, M.J., Barker, P.F., Barrett, P.J., Bowman, V., Davies, B., Smellie, J.L., Tranter, M. (Eds.), *Antarctic Paleoenvironments and Earth–Surface Processes*. Geol. Soc. London, Spec. Pub. 381, pp. 167–181.
- Kemp, A.E.S., eds., 1996, *Palaeoclimatology and Palaeoceanography from Laminated Sediments*. Geol. Soc. London, Spec. Pub. 116, 258 pp.
- Khim, B.K., Colizza, E., Lee, J.I., Giglio, F., Ha, S., Bak, Y.S., 2021. Biological productivity and glaciomarine sedimentation in the Central Basin of the northwestern Ross Sea. *Polar Sci.* 28, Article 100682.
- Kim, S., De Santis, L., Hong, J.K., Cottlerle, D., Petronio, L., Colizza, E., Kim, Y.G., Kang, S.G., Kim, H.J., Kim, S., Wardell, N., Geletti, R., Bergamasco, A., McKay, R., Jin, Y.K., Kang, S.H., 2018. Seismic stratigraphy of the

- Central Basin in northwestern Ross Sea slope and rise, Antarctica: Clues to the late Cenozoic ice-sheet dynamics and bottom-current activity. *Mar. Geol.* 395, 363–379.
- Lee, J.I., McKay, R.M., Golledge, N.R., Yoon, H.I., Yoo, K.C., Kim, H.J., Hong, J.K., 2017. Widespread persistence of expanded East Antarctic glaciers in the southwest Ross Sea during the last deglaciation. *Geology* 45, 403–406.
- Leventer, A., Domack, E., Dunbar, R., Pike, J., Stickley, C., Maddison, E., Brachfeld, S., Manley, P., McClennen, C., 2006. Marine sediment record from the East Antarctic margin reveals dynamics of ice sheet recession. *Geol. Soc. Am. Today* 16, 4–10.
- Lucchi, R.G., Rebesco, M., 2007. Glacial contourites on the Antarctic Peninsula margin: insight for palaeoenvironmental and palaeoclimatic conditions. In: Viana, A.R., Rebesco, M. (Eds.), *Economic and Palaeoceanographic Significance of Contourite Deposits*. Geol. Soc. London, Spec. Pub. 276, pp. 111–127.
- Maddison, E.J., Pike, J., Dunbar, R., 2012. Seasonally laminated diatom-rich sediments from Dumont d’Urville Trough, East Antarctic Margin: Late-Holocene Neoglacial sea-ice conditions. *The Holocene* 22, 857–875.
- Mulder, T., Syvitski, J.P.M., Migeon, S., Faugere, J.C., Savoye, B., 2003. Marine hyperpycnal flows: initiation, behavior and related deposits. A review. *Mar. Petrol. Geol.* 20, 861–882.
- Ohneiser, C., Yoo, K.C., Albot, O.B., Cortese, G., Riesselman, C., Lee, J.I., McKay, R., Bollen, M., Lee, M.K., Moon, H.S., Kim, S., Beltran, C., Levy, R., Wilson, G., 2019. Magneto-biostratigraphic age models for Pleistocene sedimentary records from the Ross Sea. *Glob. Planet. Ch.* 176, 36–49.
- Pike, J., Kemp, A.E.S., 1996. Preparation and analysis techniques for studies of laminated sediments. In: Kemp, A.S.E. (Eds.), *Palaeoclimatology and Palaeoceanography from Laminated Sediments*. Geol. Soc. London, Spec. Pub. 116, pp. 37–48.
- Pudsey, C.J., 2000. Sedimentation on the continental rise west of the Antarctic Peninsula over the last three glacial cycles. *Mar. Geol.* 167, 313–338.
- Smith, J.A., Graham, A.G.C., Post, A.L., Hillenbrand, C.D., Bart, P.J., Powell, R.D., 2019. The marine geological imprint of Antarctic ice shelves. *Nature*

- Comm. 10, 5635, doi.org/10.1038/s41467-019-13496-5
- Sprenk, D., Weber, M.E., Kuhn, G., Wennrich, V., Hartmann, T., Seelos, K., 2014. Seasonal changes in glacial polynya activity inferred from Weddell Sea varves. *Clim. the Past* 10, 1239–1251.
- Stickley, C.E., Pike, J., Leventer, A., Dunbar, R., Domack, E.W., Brachfeld, S., Manley, P., McClennan, C., 2005. Deglacial ocean and climate seasonality in laminated diatom sediments, Mac. Robertson Shelf, Antarctica. *Palaeogeogr. Palaeoclimatol. Palaeoecol.* 227, 290–310.
- Tripsanas, E.K., Piper, D.J.W., 2008. Late Quaternary stratigraphy and sedimentology of Orphan Basin: Implications for meltwater dispersal in the southern Labrador Sea. *Palaeogeogr. Palaeoclimatol. Palaeoecol.* 260, 521–539.
- Venuti, A., Florindo, F., Caburlotto, A., Hounslow, M.W., Hillenbrand, C.D., Strada, E., Talarico, F.M., Cavallo, A., 2011. Late Quaternary sediments from deep-sea sediment drifts on the Antarctic Peninsula Pacific margin: Climatic control on provenance of minerals. *J. Geophys. Res. (Solid Earth)*, 116, B06104, doi:10.1029/2010JB007952.
- Wu, L., Wang, R., Xia, W., Ge, S., Chen, Z., Krijgsman, W., 2017. Productivity–climate coupling recorded in Pleistocene sediments off Prydz Bay (East Antarctica): *Palaeogeogr. Palaeoclimatol. Palaeoecol.* 485, 260–270.

## 2 절. Glaciomarine sediment deposition on the continental slope and rise of the central Ross Sea since the Last Glacial Maximum

- Altabet, M.A., 1996. Nitrogen and carbon isotopic tracers of the source and transformation of particles in the deep Sea. In: Ittekkot, V., Schafer, P., Honjo, S., and Depetris, P.J. (Eds.), *Particle Flux in the Ocean*. John Wiley and Sons, New York, pp. 155–184.
- Altabet, M.A., Francois, R., Murray, D.W., Prell, W.L., 1995. Climate-related variations in denitrification in the Arabian Sea from sediment  $^{15}\text{N}/^{14}\text{N}$  ratios. *Nature*, 373, 506–509.
- Anderson, J.B., 1975. Factors controlling  $\text{CaCO}_3$  dissolution in the Weddell Sea

- from foraminiferal distribution patterns. *Marine Geology*, 19, 315–332.
- Anderson, J.B., Brake, C.F., Myers, N.C., 1984 Sedimentation on the Ross Sea continental shelf, Antarctica. *Marine Geology*, 57, 295–333.
- Anderson, J.B., Conway, H., Bart, P.J., Witus, A.E., Greenwood, S.L., McKay, R.M., Hall B.L., Ackert, R.P., Licht, K., Jakobsson, M., Stone, J.O., 2014. Ross Sea paleo-ice sheet drainage and deglacial history during and since the LGM. *Quaternary Science Reviews*, 100, 31–54.
- Anderson, J.B., Kurtz, D.D., Domack, E.W., Balshaw, K.M., 1980. Glacial and glacial marine sediments of the Antarctic continental shelf. *Journal of Geology*, 88, 399–414.
- Anderson, J.B., Shipp, S.S., Lowe, A.L., Wellner, J.S., Mosola, A.B. 2002. The Antarctic Ice Sheet during the Last Glacial Maximum and its subsequent retreat history: a review. *Quaternary Science Reviews*, 21, 49–70.
- Anderson, J.B., Simkins, L.M., Bart, P.J., De Santis, L., Halberstadt, A.R.W., Olivo, E., Greenwood, S.L., 2019. Seismic and geomorphic records of Antarctic Ice Sheet evolution in the Ross Sea and controlling factors in its behaviour. In: Le Heron, D.P., Hogan, K.A., Phillips, E.R., Huuse, M., Busfield, M.E., Graham, A.G.C. (Eds.), *Glaciated Margins: The Sedimentary and Geophysical Archive*. Geological Society, London, Special Publications, vol. 475, pp. 223–240.
- Andrews, J.T., Domack, E.W., Cunningham, W.L., Leventer, A., Licht, K.J., Jull, A.T., DeMaster, D.J., Jennings, A.E., 1999. Problems and possible solutions concerning radiocarbon dating of surface marine sediments, Ross Sea, Antarctica. *Quaternary Research*, 52, 206–216.
- Arrigo, K.R., van Dijken, G.L., 2004. Annual changes in sea-ice, chlorophyll *a*, and primary production in the Ross Sea, Antarctica. *Deep-Sea Research II*, 51, 117–138.
- Arrigo, K.R., DiTullio, G.R., Dunbar, R.B., Robinson, D.H., VanWoert, M., Worthen, D.L., Lizotte, M.P., 2000. Phytoplankton taxonomic variability in nutrient utilization and primary production in the Ross Sea. *Journal of Geophysical Research (Oceans)*, 105, 8827–8846.
- Barker, P.F., Barrett, P.J., Cooper, A.K., Huybrechts, P., 1999. Antarctic glacial history from numerical models and continental margin sediments.



- Palaeogeography, Palaeoclimatology, Palaeoecology, 150, 247–267.
- Bart, P.J., DeCesare, M., Rosenheim, B.E., Majewski, W., McGlannan, A., 2018. A centuries-long delay between a paleo-ice-shelf collapse and grounding-line retreat in the Whales Deep Basin, eastern Ross Sea, Antarctica. *Scientific Reports*, 8, 1–9.
- Bart, P.J., Krogmeier, B.J., Bart, M.P., Tulaczyk, S., 2017. The paradox of a long grounding during West Antarctic Ice Sheet retreat in Ross Sea. *Scientific Reports*, 7, 1–8.
- Bonaccorsi, R., Brambati, A., Busetti, M., Fanzutti, G.P., 2000. Relationship Among X-Ray Lithofacies, Magnetic Susceptibility, P-Wave Velocity and Bulk Density in Core ANTA95-89C (Ross Sea, Antarctica): First Results. *Terra Antarctica Reports*, 4, 185–198.
- Brambati, A., Fanzutti, G.P., Finocchiaro, F., Melis, R., Frignani, M., Ravaioli, M., Setti, M., 1997. Paleoenvironmental Record in Core Anta91-30 (Drygalski Basin, Ross Sea, Antarctica). In: Barker, P.F. and Cooper, A.K. (Eds.), *Geology and Seismic Stratigraphy of the Antarctic Margin 2. Antarctic Research Series vol. 71*, American Geophysical Union, pp. 137–151.
- Caburlotto, A., Lucchi, R.G., De Santis, L., Macri, P., Tolotti, R., 2010. Sedimentary processes on the Wilkes Land continental rise reflect changes in glacial dynamic and bottom water flow. *International Journal of Earth Sciences*, 99, 909–926.
- Castagno, P., Capozzi, V., DiTullio, G.R., Falco, P., Fusco, G., Rintoul, S.R., Spezie, G., Budillon, G., 2019. Rebound of shelf water salinity in the Ross Sea. *Nature Communications*, 10, 1–6.
- Ceccaroni, L., Frank, M., Frignani, M., Langone, L., Ravaioli, M., Mangini, A., 1998. Late Quaternary fluctuations of biogenic component fluxes on the continental slope of the Ross Sea, Antarctica. *Journal of Marine Systems*, 17, 515–525.
- Conte, R., Rebesco, M., De Santis, L., Colleoni, F., Bensi, M., Bergamasco, A., Kovacevic, V., Gales, J., Zgur, F., Accettella, D., De Steur, L., Ursella, L., McKay, R., Kim, S., Lucchi, R.G., IODP Expedition 374 Scientists, 2021. Bottom current control on sediment deposition between the Iselin Bank and the Hillary Canyon (Antarctica) since the late Miocene: An integrated

- seismic-oceanographic approach. *Deep Sea Research Part I: Oceanographic Research Papers*, 176, 103606.
- Cozzi, S., Cantoni, C., 2011. Stable isotope ( $\delta^{13}\text{C}$  and  $\delta^{15}\text{N}$ ) composition of particulate organic matter, nutrients and dissolved organic matter during spring ice retreat at Terra Nova Bay. *Antarctic Science*, 23, 43–56.
- Cunningham, W.L., Leventer, A., 1998. Diatom assemblages in surface sediments of the Ross Sea: relationship to present oceanographic conditions. *Antarctic Science*, 10, 134–146.
- Cunningham, W.L., Leventer, A., Andrews, J.T., Jennings, A.E., Licht, K.J., 1999. Late Pleistocene–Holocene marine conditions in the Ross Sea, Antarctica: evidence from the diatom record. *The Holocene*, 9, 129–139.
- DeConto, R.M., Pollard, D., 2016. Contribution of Antarctica to past and future sea-level rise. *Nature*, 531, 591–597.
- DeMaster, D.J., 1981. The supply and accumulation of silica in the marine environment. *Geochimica et Cosmochimica Acta*, 45, 1715–1732.
- DeNiro, M.J., Epstein, S., 1981. Influence of diet on the distribution of nitrogen isotopes in animals. *Geochimica et Cosmochimica Acta*, 45, 341–351.
- Domack, E.W., Jacobson, E. A., Shipp, S., Anderson, J.B., 1999. Late Pleistocene–Holocene retreat of the West Antarctic Ice–Sheet system in the Ross Sea: Part 2—sedimentologic and stratigraphic signature. *Geological Society of America Bulletin*, 111, 1517–1536.
- Escutia, C., Eitrem, S.L., Cooper, A.K., Nelson, C.H., 1997. Cenozoic glaciomarine sequences on the Wilkes Land continental rise, Antarctica. In: Ricci, C.A. (Eds.), *The Antarctic region: geological evolution and processes, Proceedings of the International Symposium on Antarctic Earth Sciences 7*, pp. 791–795.
- Francois, R., Altabet, M.A., Burckle, L.H., 1992. Glacial to interglacial changes in surface nitrate utilization in the Indian sector of the Southern Ocean as recorded by sediment  $\delta^{15}\text{N}$ . *Paleoceanography*, 7, 589–606.
- Fretwell, P., Pritchard, H. D., Vaughan, D. G., Bamber, J. L., Barrand, N. E., Bell, R., Bianchi, C., Bingham, R.G., Blankenship, D.D., Casassa, G., Catania, G., Callens, D., Conway, H., Cook, A.J., Corr1, H.F.J., D. Damaske, D., Damm, V., Ferraccioli, F., Forsberg, R., Fujita, S., Gogineni, P., Griggs,

- J.A., Hindmarsh, R.C.A., Holmlund, P., Holt, J.W., Jacobel, R.W., Jenkins, A., Jokat, W., Jordan, T., King, E.C., Kohler, J., Krabill, W., Riger-Kusk, M., Langley, K.A., Leitchenkov, G., Leuschen, C., Luyendyk, B.P., Matsuoka, K., Nogi, Y., Nost, O.A., Popov, S.V., Rignot, E., Rippin, D.M., Riviera, A., Roberts, J., Ross, N., Siegert M.J., Smith, A.M., Steinhage, D., Studinger, M., Sun, B., Tinto, B.K., Welch, B.C., Young, D.A., Xiangbin, C., Zirizzotti, A., 2013. Bedmap2: improved ice bed, surface and thickness datasets for Antarctica. *The Cryosphere*, 7, 375–393.
- Friedman, G.M., Sanders, J.E., 1978. *Principles of Sedimentology*. John Wiley and Sons. New York.
- Frignani, M., Giglio, F., Langone, L., Ravaioli, M., Mangini, A., 1998. Late Pleistocene–Holocene sedimentary fluxes of organic carbon and biogenic silica in the northwestern Ross Sea, Antarctica. *Annals of Glaciology*, 27, 697–703.
- Gales, J., Rebesco, M., De Santis, L., Bergamasco, A., Colleoni, F., Kim, S., Accettella, D., Kovacevic, V., Liu, Y., Olivo, E., Colizza, E., Florindo-Lopez, C., Zgur, F., McKay, R., 2021. Role of dense shelf water in the development of Antarctic submarine canyon morphology. *Geomorphology*, 372, 107453.
- Gilbert, I.M., Pudsey, C.J., Murray, J.W., 1998. A sediment record of cyclic bottom-current variability from the northwest Weddell Sea. *Sedimentary Geology*, 115, 185–214.
- Golledge, N.R., Levy, R.H., McKay, R.M., Fogwill, C.J., White, D.A., Graham, A.G.C., Smith, J.A., Hillenbrand, C.-D., Licht, K.J., Denton, G.H., Ackert, R.P., Maas, S.M., Hall, B.L., 2013. Glaciology and geological signature of the Last Glacial Maximum Antarctic ice sheet. *Quaternary Science Reviews*, 78, 225–247.
- Govin, A., Michel, E., Labeyrie, L., Waelbroeck, C., Dewilde, F., & Jansen, E. (2009). Evidence for northward expansion of Antarctic Bottom Water mass in the Southern Ocean during the last glacial inception. *Paleoceanography*, 24, PA1202, <https://doi.org/10.1029/2008PA001603>.
- Grobe, H., Mackensen, A., 1992. Late Quaternary climatic cycles as recorded in sediments from the Antarctic continental margin. In: Kennett, J.P., Warnke,

- D.A. (Eds.), *The Antarctic Paleoenvironment: A Perspective on Global Change: Part One*. Antarctic Research Series vol. 56, American Geophysical Union, pp. 349–376.
- Ha, S., Khim, B.K., Cho, H.G., Colizza, E., 2018. Origin of clay minerals of core RS14-GC2 in the continental slope to the east of the Pennell–Iselin Bank in the Ross Sea, Antarctica. *Journal of Mineralogical Society of Korea*, 31, 1–12. (in Korean with English abstract)
- Halberstadt, A.R.W., Simkins, L.M., Greenwood, S.L., Anderson, J.B., 2016. Past ice-sheet behaviour: retreat scenarios and changing controls in the Ross Sea, Antarctica. *The Cryosphere*, 10, 1003–1020.
- Hall, B.L., Henderson, G.M., Baroni, C., Kellogg, T.B., 2010. Constant Holocene Southern-Ocean  $^{14}\text{C}$  reservoir ages and ice-shelf flow rates. *Earth and Planetary Science Letters*, 296, 115–123.
- Hartman, J. D., Sangiorgi, F., Barcena, M. A., Tateo, F., Giglio, F., Albertazzi, S., Trincardi, F., Bijl, P.K., Langone, L., Asioli, A., 2021. Sea-ice, primary productivity and ocean temperatures at the Antarctic marginal zone during late Pleistocene. *Quaternary Science Reviews*, 266, 107069.
- Heaton, T. J., Köhler, P., Butzin, M., Bard, E., Reimer, R. W., Austin, W. E., Bronk, R.C., Grootes, P.M., Hughen, K.A., Kromer, B., Reimer, P.J., Adkins, J., Burke, A., Cook, M.S., Olsen, J., Skinner, L.C., 2020. Marine20—the marine radiocarbon age calibration curve (0–55,000 cal BP). *Radiocarbon*, 62, 779–820.
- Hillenbrand, C.D., Crowhurst, S.J., Williams, M., Hodell, D.A., McCave, I.N., Ehrmann, W., Xuan, C., Piotrowski, A.M., Hernández–Molin, F.J., Graham, A.G.C., Grobe, H., Williams, T.J., Horrocks, J.R., Allen, C.S., Larter, R.D., 2021. New insights from multi-proxy data from the West Antarctic continental rise: Implications for dating and interpreting Late Quaternary palaeoenvironmental records. *Quaternary Science Reviews*, 257, 106842
- Hillenbrand, C.D., Smith, J.A., Kuhn, G., Esper, O., Gersonde, R., Larter, R.D., Maher, B., Moreton, S.G., Shimmield, T.M., Korte, M., 2010. Age assignment of a diatomaceous ooze deposited in the western Amundsen Sea Embayment after the Last Glacial Maximum. *Journal of Quaternary Science*, 25, 280–295.

- Howat, I.M., Domack, E.W., 2003. Reconstructions of western Ross Sea palaeo-ice-stream grounding zones from high-resolution acoustic stratigraphy. *Boreas*, 32, 56–75.
- Jacobs, S.S., 2004. Bottom water production and its links with the thermohaline circulation. *Antarctic Science*, 16, 427–437.
- Khim, B.K., Colizza, E., Lee, J.I., Giglio, F., Ha, S., Bak, Y.S., 2021. Biological productivity and glaciomarine sedimentation in the Central Basin of the northwestern Ross Sea since the last glacial maximum. *Polar Science*, 28, 100682.
- Kim, S., Lee, J.I., McKay, R.M., Yoo, K.C., Bak, Y.S., Lee, M.K., Roh, Y.H., Yoon, H.I., Moon H.S., Hyun, C.U., 2020. Late Pleistocene paleoceanographic changes in the Ross Sea–Glacial–interglacial variations in paleoproductivity, nutrient utilization, and deep–water formation. *Quaternary Science Reviews*, 239, 106356.
- King, M.V., Gales, J.A., Laberg, J.S., McKay, R.M., De Santis, L., Kulhanek, D.K., Hosegood, P.J., Morris, A., Expedition, I.O.D.P., 2022. Pleistocene depositional environments and links to cryosphere–ocean interactions on the eastern Ross Sea continental slope, Antarctica (IODP Hole U1525A). *Marine Geology*, 443, 106674.
- Kristensen, E., Blackburn, T.H., 1987. The fate of organic carbon and nitrogen in experimental marine sediment systems: influence of bioturbation and anoxia. *Journal of Marine Research*, 45, 231–257.
- Kuvaas, B., Leitchenkov, G., 1992. Glaciomarine turbidite and current controlled deposits in Prydz Bay, Antarctica. *Marine Geology*, 108, 365–381.
- Langone, L., Frignani, M., Labbrozzi, L., Ravaioli, M., 1998. Present-day biosiliceous sedimentation in the northwestern Ross Sea, Antarctica. *Journal of Marine Systems*, 17, 459–470.
- Langone, L., Frignani, M., Ravaioli, M., Bianchi, C., 2000. Particle fluxes and biogeochemical processes in an area influenced by seasonal retreat of the ice margin (northwestern Ross Sea, Antarctica). *Journal of Marine Systems*, 27, 221–234.
- Larter, R.D., Barker, P.F., 1989. Seismic stratigraphy of the Antarctic Peninsula Pacific margin: A record of Pliocene–Pleistocene ice volume and

- paleoclimate. *Geology*, 17, 731–734.
- Ledford–Hoffman, P.A., DeMaster, D.J., Nittrouer, C.A., 1986. Biogenic–silica accumulation in the Ross Sea and the importance of Antarctic continental–shelf deposits in the marine silica budget. *Geochimica et Cosmochimica Acta*, 50, 2099–2110.
- Licht, K.J., Dunbar, N.W., Andrews, J.T., Jennings, A.E., 1999. Distinguishing subglacial till and glacial marine diamictos in the western Ross Sea, Antarctica: Implications for a last glacial maximum grounding line. *Geological Society of America Bulletin*, 111, 91–103.
- Licht, K.J., Jennings, A.E., Andrews, J.T., Williams, K.M., 1996. Chronology of late Wisconsin ice retreat from the western Ross Sea, Antarctica. *Geology*, 24, 223–226.
- Licht, K.J., Lederer, J.R., Swope, R.J., 2005. Provenance of LGM glacial till (sand fraction) across the Ross embayment, Antarctica. *Quaternary Science Reviews*, 24, 1499–1520.
- Livingstone, S.J., Cofaigh, C.Ó., Stokes, C.R., Hillenbrand, C.D., Vieli, A., Jamieson, S.S., 2012. Antarctic palaeo–ice streams. *Earth–Science Reviews*, 111, 90–128.
- Lowry, D.P., Golledge, N.R., Bertler, N.A., Jones, R.S., McKay, R., Stutz, J., 2020. Geologic controls on ice sheet sensitivity to deglacial climate forcing in the Ross Embayment, Antarctica. *Quaternary Science Advances*, 1, 100002.
- Lucchi, R. G., Rebesco, M., 2007. Glacial contourites on the Antarctic Peninsula margin: insight for palaeoenvironmental and palaeoclimatic conditions. In: Viana, A.L. and Rebesco, M. (Eds.), *Economic and Paleoceanographic Significance of Contourite Deposits*. Geological Society of London, Special Publications, vol. 276, pp. 111–127.
- Mackensen, A., 2004. Changing Southern Ocean palaeocirculation and effects on global climate. *Antarctic Science*, 16, 369–386.
- Martin, S., 2001. Polynyas. In: Steele, J.H., Thorpe, S.A., and Turekian, K.K. (Eds.), *Encyclopedia of Ocean Sciences*. Academic Press, San Diego, pp. 2241–2247.
- McCave, I.N., Andrews, J.T., 2019. Distinguishing current effects in sediments delivered to the ocean by ice. I. Principles, methods and examples.

- Quaternary Science Reviews, 212, 92–107.
- McGlannan, A.J., Bart, P.J., Chow, J.M., DeCesare, M., 2017. On the influence of post-LGM ice shelf loss and grounding zone sedimentation on West Antarctic ice sheet stability. *Marine Geology*, 392, 151–169.
- McKay, R.M., Dunbar, G.B., Naish, T.R., Barrett, P.J., Carter, L., Harper, M., 2008. Retreat history of the Ross Ice Sheet (Shelf) since the Last Glacial Maximum from deep-basin sediment cores around Ross Island. *Palaeogeography, Palaeoclimatology, Palaeoecology*, 260, 245–261.
- Melis, R., Capotondi, L., Torricella, F., Ferretti, P., Geniram, A., Hong, J.K., Kuhn, G., Khim, B.K., Kim, S., Malinverno, E., Yoo, K.C., Colizza, E. 2021. Last Glacial Maximum to Holocene paleoceanography of the northwestern Ross Sea inferred from sediment core geochemistry and micropaleontology at Hallett Ridge. *Journal of Micropalaeontology*, 40, 15–35.
- Melis, R., Salvi, G., 2009. Late Quaternary foraminiferal assemblages from western Ross Sea (Antarctica) in relation to the main glacial and marine lithofacies. *Marine Micropaleontology*, 70, 39–53.
- Meyers, P.A., 1994. Preservation of elemental and isotopic source identification of sedimentary organic matter. *Chemical Geology*, 114, 289–302.
- Mezgec, K., Stenni, B., Crosta, X., Masson-Delmotte, V., Baroni, C., Braidà, M., Ciardini, V., Colizza, E., Melis, M., Salvatore, C., Severi, M., Scarchilli, C., Traversi, R., Udisti, R., Frezzotti, M., 2017. Holocene sea ice variability driven by wind and polynya efficiency in the Ross Sea. *Nature Communications*, 8, 1–12.
- Mollenhauer, G., Grotheer, H., Gentz, T., Bonk, E., and Hefter, J., 2021. Standard operation procedures and performance of the MICADAS radiocarbon laboratory at Alfred Wegener Institute (AWI), Germany. *Nuclear Instruments and Methods in Physics Research Section B: Beam Interactions with Materials and Atoms*, 496: 45–51
- Mortlock, R.A., Froelich, P.N., 1989. A simple method for the rapid determination of biogenic opal in pelagic marine sediments. *Deep-Sea Research A*, 36, 1415–1426.
- Mosola, A.B., Anderson, J.B., 2006. Expansion and rapid retreat of the West Antarctic Ice Sheet in eastern Ross Sea: possible consequence of

- over-extended ice streams? *Quaternary Science Reviews*, 25, 2177–2196.
- Nakada, M., Kimura, R., Okuno, J., Moriwaki, K., Miura, H., Maemoku, H. 2000. Late Pleistocene and Holocene melting history of the Antarctic ice sheet derived from sea-level variations. *Marine Geology*, 167, 85–103.
- O'Brien, P.E., Post, A.L., Edwards, S., Martin, T., Caburlotto, A., Donda, F., Leitchenkov, G., Romeo, R., Duffy, M., Evangelinos, D., Holder, L., Leventer, A., López-Quirós, A., Opdyke, B.N. Armand, L.K., 2020. Continental slope and rise geomorphology seaward of the Totten Glacier, East Antarctica (112°E–122°E). *Marine Geology*, 427, 106221.
- Ó Cofaigh, C., Dowdeswell, J.A., Pudsey, C.J., 2001. Late Quaternary iceberg rafting along the Antarctic Peninsula continental rise and in the Weddell and Scotia Seas. *Quaternary Research*, 56, 308–321.
- Ogura, T.O., Abe-Ouchi, A., 2001. Influence of the Antarctic ice sheet on southern high latitude climate during the Cenozoic: Albedo vs topography effect. *Geophysical Research Letters*, 28, 587–590.
- Pattyn, F., Ritz, C., Hanna, E., Asay-Davis, X., DeConto, R., Durand, G., Favier, L., Fettweis, X., Goelzer, H., Gollledge, N.R., Munneke, P.K., Lenaerts, J.T.M., Nowicki, S., Payne, A.J., Robinson, A., Seroussi, H., Trusel, L.D., Van den Broeke, M., 2018. The Greenland and Antarctic ice sheets under 1.5°C global warming. *Nature Climate Change*, 8, 1053–1061.
- PNRA-ENEA/UTA, 2014. Rapporto sulla Campagna Antartica –Estate Australe 2013–2014 – XXIX spedizione. ISSN 17232–7084, 212 pp.
- Prothro, L.O., Majewski, W., Yokoyama, Y., Simkins, L.M., Anderson, J.B., Yamane, M., Miyairi, Y., Ohkouchi, N., 2020. Timing and pathways of east Antarctic ice sheet retreat. *Quaternary Science Reviews*, 230, 106166.
- Prothro, L.O., Simkins, L.M., Majewski, W., Anderson, J.B., 2018. Glacial retreat patterns and processes determined from integrated sedimentology and geomorphology records. *Marine Geology*, 395, 104–119.
- Pudsey, C.J., 1992. Late Quaternary changes in Antarctic Bottom Water velocity inferred from sediment grain size in the northern Weddell Sea. *Marine Geology*, 107, 9–33.
- Pudsey, C.J., 2000. Sedimentation on the continental rise west of the Antarctic Peninsula over the last three glacial cycles. *Marine Geology*, 167, 313–338.



- Pudsey, C.J., Camerlenghi, A., 1998. Glacial–interglacial deposition on a sediment drift on the Pacific margin of the Antarctic Peninsula. *Antarctic Science*, 10, 286–308.
- Pudsey, C.J., Murray, J.W., Appleby, P., Evans, J., 2006. Ice shelf history from petrographic and foraminiferal evidence, Northeast Antarctic Peninsula. *Quaternary Science Reviews*, 25, 2357–2379.
- Rau, G.H., Froelich, P.N., Takahashi, T.D., Des Marais, D.J., 1991. Does sedimentary organic  $\delta^{13}\text{C}$  record variations in Quaternary ocean [ $\text{CO}_{2(\text{aq})}$ ]? *Paleoceanography*, 6, 335–347.
- Rau, G.H., Riebesell, U., Wolf-Gladrow, D., 1997.  $\text{CO}_{2(\text{aq})}$ -dependent photosynthetic  $^{13}\text{C}$  fractionation in the ocean: A model versus measurements. *Global Biogeochemical Cycles*, 11, 267–278.
- Reimer, P. J., Bard, E., Bayliss, A., Beck, J. W., Blackwell, P. G., Ramsey, C. B., Buck, C., Cheng, H., Edwards, L. Friedrich, M., Grootes P.M., Guilderson, T.P., Hafflidason, G., Hajdas, I., Hatte, C., Heaton, T.J., Hoffmann, D.L., Hogg, A.G., Hughen, K.A., Kaiser, K.F., Kromer, B., Manning, S.W., Niu, M., Reimer, R.W., Richards, D.A., Scott, E.M., Southon, J.R., Staff, R.A., Turney, C.S.M., Van Der Plicht, J., 2013. IntCal13 and Marine13 radiocarbon age calibration curves 0–50,000 years cal BP. *Radiocarbon*, 55, 1869–1887.
- Rignot, E., Bamber, J.L., Van Den Broeke, M.R., Davis, C., Li, Y., Van De Berg, W.J., Van Meijgaard, E., 2008. Recent Antarctic ice mass loss from radar interferometry and regional climate modelling. *Nature Geoscience*, 1, 106–110.
- Ritz, C., Edwards, T.L., Durand, G., Payne, A.J., Peyaud, V., Hindmarsh, R.C., 2015. Potential sea-level rise from Antarctic ice-sheet instability constrained by observations. *Nature*, 528, 115–118.
- Robinson, R.S., Sigman, D.M., 2008. Nitrogen isotopic evidence for a poleward decrease in surface nitrate within the ice age Antarctic. *Quaternary Science Reviews*, 27, 1076–1090.
- Salvi, C., Busetti, M., Marinoni, L., Brambati, A., 2006. Late Quaternary glacial marine to marine sedimentation in the Pennell Trough (Ross Sea, Antarctica). *Palaeogeography, Palaeoclimatology, Palaeoecology*, 231,

199–214.

- Shipp, S., Anderson, J.B., Domack, E.W., 1999. Seismic signature of the Late Pleistocene fluctuation of the West Antarctic Ice Sheet system in Ross Sea: a new perspective, Part I. *Geological Society of America Bulletin*, 111, 1486–1516.
- Smith, J.A., Graham, A.G., Post, A.L., Hillenbrand, C.D., Bart, P.J., Powell, R.D., 2019. The marine geological imprint of Antarctic ice shelves. *Nature Communications*, 10, 1–16.
- Smith, J.A., Hillenbrand, C.D., Pudsey, C.J., Allen, C.S., Graham, A.G., 2010. The presence of polynyas in the Weddell Sea during the Last Glacial Period with implications for the reconstruction of sea-ice limits and ice sheet history. *Earth and Planetary Science Letters*, 296, 287–298.
- Smith Jr, W.O., Ainley, D.G., Arrigo, K.R., Dinniman, M.S., 2014. The oceanography and ecology of the Ross Sea. *Annual Review of Marine Science*, 6, 469–487.
- Stow, D., Smillie, Z., 2020. Distinguishing between deep-water sediment facies: Turbidites, contourites and hemipelagites. *Geosciences*, 10, 68.
- Stuiver, M., Reimer, P.J., Reimer, R.W., 2018. CALIB 7.1. 2017. URL: <http://calib.org> (accessed: 30.11. 2017).
- Tesi, T., Belt, S. T., Gariboldi, K., Muschitiello, F., Smik, L., Finocchiaro, F., Giglio, F., Colizza, E., Gazzurra, G., Giordano, P., Morigi, C., Capotondi, L., Nogarotto, A., Köseoğlu, D., Roberto, A.D., Gallerani A., Langone, L., 2020. Resolving sea ice dynamics in the north-western Ross Sea during the last 2.6 ka: From seasonal to millennial timescales. *Quaternary Science Reviews*, 237, 106299.
- Thompson, A.F., Stewart, A.L., Spence, P., Heywood, K.J., 2018. The Antarctic Slope Current in a changing climate. *Reviews of Geophysics*, 56, 741–770.
- Tolotti, R., Salvi, C., Salvi, G., Bonci, M.C., 2013. Late Quaternary climate variability as recorded by micropalaeontological diatom data and geochemical data in the western Ross Sea, Antarctica. *Antarctic Science*, 25, 804–820.
- Tooze, S., Halpin, J.A., Noble, T.L., Chase, Z., O'Brien, P.E., Armand, L., 2020. Scratching the surface: a marine sediment provenance record from the

- continental slope of central Wilkes Land, East Antarctica. *Geochemistry, Geophysics, Geosystems*, 21, e2020GC009156.
- Torricella, F., Melis, R., Malinverno, E., Fontolan, G., Bussi, M., Capotondi, L., Carlo, P.D., Roberto, A.D., Geniram, A., Kuhn, G., Khim, B.K., Morigi, C., Scateni, B., Colizza, E., 2021. Environmental and Oceanographic Conditions at the Continental Margin of the Central Basin, Northwestern Ross Sea (Antarctica) Since the Last Glacial Maximum. *Geosciences*, 11, 155.
- Villinski, J.C., Dunbar, R.B., Mucciarone, D.A., 2000. Carbon 13/Carbon 12 ratios of sedimentary organic matter from the Ross Sea, Antarctica: A record of phytoplankton bloom dynamics. *Journal of Geophysical Research (Oceans)*, 105, 14163–14172.
- Wacker, L., Fahrni, S.M., Hajdas, I., Molnar, M., Synal, H.A., Szidat, S., Zhang, Y.L., 2013. A versatile gas interface for routine radiocarbon analysis with a gas ion source. *Nuclear Instruments and Methods in Physics Research Section B: Beam Interactions with Materials and Atoms*, 294, 315–319.
- Weber, M.E., Bonani, G., Fütterer, K.D., 1994. Sedimentation processes within channel-ridge systems, southeastern Weddell Sea, Antarctica. *Paleoceanography*, 9, 1027–1048.
- Weber, M.E., Clark, P.U., Ricken, W., Mitrovica, J.X., Hostetler, S.W., Kuhn, G., 2011. Interhemispheric ice-sheet synchronicity during the Last Glacial Maximum. *Science*, 334, 1265–1269.
- Weber, M.E., Clark, P.U., Kuhn, G., Timmermann, A., Spreng, D., Gladstone, R., Zhang, X., Lohmann, G., Menviel, L., Chikamoto, M.O., Friedrich, T., Ohlwein, C., 2014. Millennial-scale variability in Antarctic ice-sheet discharge during the last deglaciation. *Nature*, 510, 134–138.
- Yokoyama, Y., Lambeck, K., De Deckker, P., Johnston, P., Fifield, L.K., 2000. Timing of the Last Glacial Maximum from observed sea-level minima. *Nature*, 406, 713–716.

## 주 의

1. 이 보고서는 극지연구소 위탁과제 연구결과보고서입니다.
2. 이 보고서 내용을 발표할 때에는 반드시 극지연구소에서 위탁연구과제로 수행한 연구결과임을 밝혀야 합니다.
3. 국가과학기술 기밀유지에 필요한 내용은 대외적으로 발표 또는 공개하여서는 안됩니다.